SJÄLVSTÄNDIGA ARBETEN I MATEMATIK

MATEMATISKA INSTITUTIONEN, STOCKHOLMS UNIVERSITET

# Sequential differentiation of polynomials with zeros determined by simple polygons

av

**Christian Hägg**

2015 - No 23

MATEMATISKA INSTITUTIONEN, STOCKHOLMS UNIVERSITET, 106 91 STOCKHOLM

# Sequential differentiation of polynomials with zeros determined by simple polygons

Christian Hägg

---

Självständigt arbete i matematik 15 högskolepoäng, grundnivå

Handledare: Rikard Bøgvad

2015

**Abstract**

Consider a complex polynomial $P$ with simple zeros in lattice points contained in a simple polygon $\mathcal{S}$. We numerically investigate how the zeros of $P$, $P'$, $P''$, ... change, and notice that they converge on trees. By instead considering a polynomial $p$ with zeros of multiplicity $n$ in the vertices of $\mathcal{S}$, we see that the zeros of the $n$:th derivative of $p$ reside in more refined trees or forests. These organic shapes seem to, given light restrictions, be contained in unique, simple polygons on the vertices of $\mathcal{S}$.

## Acknowledgments

I am very grateful to Rikard Bögvad for suggesting that I explore how the distribution of zeros of complex polynomials changes after differentiation. His encouragement for my various experiments, such as numerical trials related to repeated differentiation, has been highly motivating, and his knowledge and insight have been wonderful resources. I would also like to thank Boris Shapiro for his ideas, suggestions, and astute insights into the nature of complex analysis. Finally, I express my gratitude to Björn Gustafsson for his keen advice, insight and corrections.

# Contents

# 1 Introduction

In 1836, Carl Friedrich Gauss (1777-1855) investigated the properties of the fields of forces generated by identical, point-shaped particles with an attractive force inversely proportional to the distance to the particle.[8] In particular, Gauss showed that if such particles are placed in the zeros of a polynomial $P$, the zeros of its derivative $P'$ that are distinct from the zeros of the original polynomial will be the points of equilibrium in the field of force (assuming $k$ particles are placed in each zero of multiplicity $k$). Gauss' results can be used to prove the Gauss-Lucas theorem (Theorem 2.1 below), which limits the geometry of the zeros of $P'$.

In this paper, we will, based on the Gauss-Lucas theorem, experimentally investigate the geometries of the zeros of $P$, $P'$, $P''$, ..., and formulate a number of conjectures about their behavior. Furthermore, we will initially focus our inquiries on polynomials $P$ with simple, regular zeros (in the Gaussian integers, for example) inside simple polygons with predetermined geometries. As we shall see later, however, condensing the zeros in the vertices of the polygons will give rise to more refined versions of the structures that emerge in the aforementioned case. Finally, we will perform a few related experiments to motivate further studies.

## 2 Theory

Before we formulate and prove the Gauss-Lucas theorem, which has been named in honor of the French engineer Félix Lucas who originally discovered and proved it in 1878, we will define the concepts of convex sets and convex hulls.

**Definition 2.1.** *A set $X$ in a real or complex vector space is convex if*

$$x_1, x_2 \in X \implies \lambda x_1 + (1-\lambda)x_2 \in X \quad \forall \quad \lambda \in [0,1]. \tag{1}$$

Consequently, a set $X$ is convex if any pair of distinct points in $X$ can be joined by a line segment that lies entirely within $X$.

**Definition 2.2.** *Let $X$ be a set in a real or complex vector space. The convex hull of $X$, denoted* $\mathrm{Conv}(X)$*, is the intersection of all convex sets which contain $X$.*

Thus, the convex hull of the set $X$ is the smallest convex set that contains $X$.

We are ready for the Gauss-Lucas theorem. The proof given relies somewhat less on geometry than many other proofs for the theorem.[2]

**Theorem 2.1** (Gauss-Lucas)**.** *Let $P$ be a non-constant polynomial in one variable. Then all the zeros of its derivative lie in the convex hull $H$ of the zeros of $P$.*

*Proof.* Let $P(z) = a_n z^n + a_{n-1} z^{n-1} + \cdots + a_1 z + a_0$ denote the polynomial, and assume that $\zeta$ is a zero of $P'$ such that $P(\zeta) \neq 0$. Furthermore, let $z_1, z_2, \ldots, z_k$ denote all distinct zeros of $P$ with multiplicities $m_1, m_2, \ldots, m_k$ respectively. Using the fundamental theorem of algebra (Theorem A.2, page 69),

$$P(z) = a_n \prod_{j=1}^{k} (z - z_j)^{m_j}. \tag{2}$$

Taking the derivative of (2) using the Leibniz product rule (Theorem A.4, page 70) followed by division by $P$ yields

$$\frac{P'(z)}{P(z)} = \sum_{j=1}^{k} \frac{m_j}{z - z_j}. \tag{3}$$

Substituting $\zeta$ in (3) yields, since $\overline{0} = 0$,

$$\begin{aligned} 0 = \frac{P'(\zeta)}{P(\zeta)} &= \sum_{j=1}^{k} \frac{m_j}{\zeta - z_j} = \overline{\sum_{j=1}^{k} \frac{m_j}{\zeta - z_j}} = \sum_{j=1}^{k} \frac{m_j}{\overline{\zeta} - \overline{z_j}} \\ &= \sum_{j=1}^{k} \frac{m_j |\zeta - z_j|^2}{(\overline{\zeta} - \overline{z_j})|\zeta - z_j|^2} = \sum_{j=1}^{k} \frac{m_j}{|\zeta - z_j|^2}(\zeta - z_j). \end{aligned} \tag{4}$$

Consequently

$$0 = \sum_{j=1}^{k} \frac{m_j}{|\zeta - z_j|^2}(\zeta - z_j) = \sum_{j=1}^{k} c_j(\zeta - z_j), \tag{5}$$

where

$$c_j := \frac{m_j}{|\zeta - z_j|^2} > 0, \quad j = 1, 2, \ldots, k. \tag{6}$$

Solving (5) for $\zeta$, we get

$$\zeta = \frac{1}{\sum_{j=1}^{k} c_j} \left( \sum_{j=1}^{k} c_j z_j \right) = \sum_{j=1}^{k} d_j z_j, \tag{7}$$

where

$$d_j := \frac{c_j}{\sum_{r=1}^{k} c_r}, \quad j = 1, 2, \ldots, k. \tag{8}$$

We note that $0 < d_j \leq 1, j = 1, 2, \ldots, k$, and $\sum_{j=1}^{k} d_j = 1$. Consequently, the weighted sum in (7) shows that $\zeta$ is in the convex hull $H$. □

**Remark 2.1.** *It can be shown that if the zeros of $P$ are not collinear, then the zeros of $P'$ lie inside the boundary of $H$, assuming that they are not multiple zeros of $P$.*[6] *Furthermore, Gauss' investigations (see Theorem A.1 on page 69) guarantee that if $P$ is a polynomial of degree $n \geq 2$ with simple zeros (of multiplicity 1), then the convex hull of its critical points is smaller than the convex hull of its zeros.*[7]

Although collinearity of zeros tends to arise when regular grids of zeros are considered, we give the following theorem, which yields some geometric intuition as to how the convex hull shrinks when the derivative of a polynomial is taken.

**Theorem 2.2.** *Let $p : \mathbb{C} \to \mathbb{C}$ be a polynomial of degree $n$ with $d$ zeros located in the interior of the convex hull of the other zeros. For each inner zero of $p$, which is not collinear with two other zeros, there is a sector defined by the inner zero and two (adjacent) rays through other zeros which does not contain a zero of $p'$.*

Proving Theorem 2.2 is a straightforward but somewhat lengthy endeavour, so we direct the interested reader to Andreas Rüdinger's paper on this particular problem.[11] An application of Theorem 2.2 is given below in Figure 1, where we investigate the zeros and critical points of the polynomial $\widehat{p} = z(z-1)(z-2)(z-i)(z-(1+i))(z-(2+i))(z-(4/5+3i/5))(z-(3/2+i/8))$.

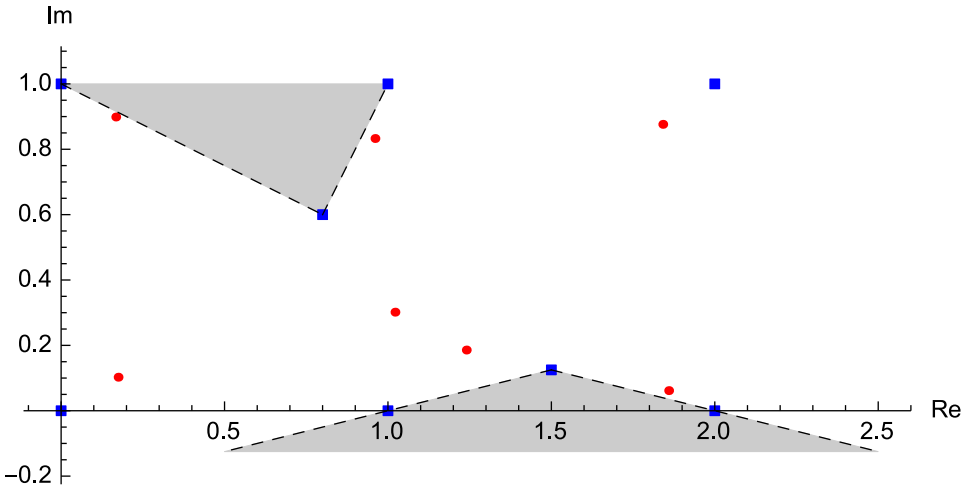


Figure 1: The zeros of the polynomial $\widehat{p}$ (squares) and its critical points (disks). Note that the two triangular sectors contain no critical points of $\widehat{p}$, in accordance with Theorem 2.2.

Unfortunately, Theorem 2.2 yields no obvious way to determine which sectors are devoid of critical points. Even in the case $n = 4$, when we have only three sectors to consider, there is no known geometric criterion to determine which sector contains no critical points.

A more explicit construction to find critical points of a polynomial $P$ is given by Linfield's theorem (Theorem 2.3) below, which requires us to define the class of a curve.[9]

**Definition 2.3.** *The class of a curve $\mathcal{C}$ is the number of tangents that can be drawn to $\mathcal{C}$ from a point not on $\mathcal{C}$, counting multiplicities and imaginary tangents.*

**Theorem 2.3** (Linfield)**.** *The zeros of the rational function*

$$R(z) := \sum_{j=1}^{k} \frac{\lambda_j}{z - z_j} \qquad (\lambda_j \in \mathbb{R} \setminus \{0\}, j = 1, \ldots, k), \tag{9}$$

*are the foci of the curve of class $k-1$ which touches each of the $k(k-1)/2$ line segments $\overline{z_\mu, z_\nu}$ in a point dividing that line segment in the ratio $\lambda_\mu : \lambda_\nu$.*

If the polynomial $P$ has distinct zeros $z_1, \ldots, z_k$, then we can, as in our proof for Theorem 2.1 above, write $P'$ on the form

$$P'(z) = P(z) \sum_{j=1}^{k} \frac{m_j}{z - z_j}, \tag{10}$$

where $m_j \geq 1$ is the multiplicity of $z_j$, $j = 1, \ldots k$. Thus, Theorem 2.3 can be used to locate the zeros of $P'$ which are not zeros of $P$. Consequently, if we consider a polynomial $P$ with only simple zeros, all zeros of $P'$ can be located by constructing such a curve.

**Example 2.1.** Let $P$ be the polynomial of degree 3 with distinct zeros $z_1, z_2$, and $z_3$ that are not collinear, and thus form the vertices of a triangle $\mathcal{T}$. To find the zeros of $P'$, we write it in the form

$$P'(z) = P(z) \sum_{j=1}^{3} \frac{1}{z - z_j}, \tag{11}$$

and seek the curve of class 2 that touches each of the three sides of $\mathcal{T}$ at their midpoints. This curve is the Steiner inellipse[12] $E$ of $\mathcal{T}$, and consequently, by Theorem 2.3, the zeros of $P'$ are the focal points of $E$. We illustrate the situation below, where the zeros of $P$ have been chosen as $z_1 = 1 + i$, $z_2 = 3 + 4i$, and $z_3 = 6 + 3i$.

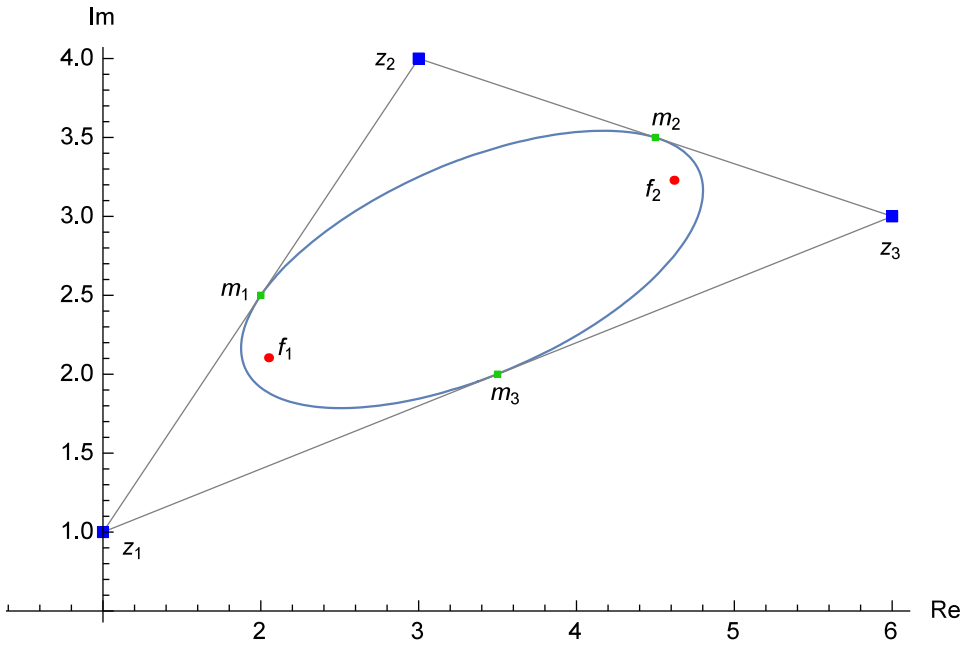


Figure 2: The polynomial $P$ with zeros $z_1$, $z_2$, and $z_3$ that make up a triangle $\mathcal{T}$ whose sides have midpoints $m_1$, $m_2$, and $m_3$. The focal points of the Steiner inellipse of $\mathcal{T}$ are $f_1$ and $f_2$, which are also the zeros of $P'$.

As we shall see in section 3.1, if $p$ is a polynomial that has only simple zeros, then $p'$ may have zeros of multiplicity $m \geq 2$. Consequently, it is possible that the convex hulls of the zeros of $p^{(k)}$ and $p^{(k+1)}$, respectively, may have intersecting boundaries, for $1 \leq k < n-1$. The following, simple theorem describes the 'resistance' of these zeros to differentiation.

**Theorem 2.4.** *Let $P$ be a polynomial with zero $z_\ell$ of multiplicity $m_\ell$. If $m_\ell \geq 2$, then $z_\ell$ is a zero of $P'$ with multiplicity $m_\ell - 1$. Otherwise, $z_\ell$ is not a zero of $P'$.*

*Proof.* Analogously to the proof for Theorem 2.1 above, we let $P(z) = a_n z^n + a_{n-1} z^{n-1} + \cdots + a_1 z + a_0$ denote the polynomial, which has $k$ distinct zeros $z_1, z_2, \ldots, z_k$ of multiplicities $m_1, m_2, \ldots, m_k$, respectively. Furthermore, $P$ can be written in the form

$$P(z) = a_n \prod_{j=1}^{k} (z - z_j)^{m_j}. \tag{12}$$

Taking the derivative of $P$, we see from equation (12) that

$$\begin{aligned} P'(z) = a_n \big[ & m_1(z-z_1)^{m_1-1}(z-z_2)^{m_2}\cdots(z-z_k)^{m_k} \\ & + m_2(z-z_1)^{m_1}(z-z_2)^{m_2-1}\cdots(z-z_k)^{m_k} + \cdots \\ & + m_k(z-z_1)^{m_1}(z-z_2)^{m_2}\cdots(z-z_k)^{m_k-1} \big]. \end{aligned} \tag{13}$$

Consider any zero $z_j$ of $P$. If $z_j$ is a simple zero, equation (13) immediately yields that

$$P'(z_j) = m_j(z_j - z_1)^{m_1}\cdots(z_j - z_{j-1})^{m_{j-1}}(z_j - z_{j+1})^{m_{j+1}}\cdots(z_j - z_k)^{m_k} \neq 0, \tag{14}$$

since the zeros are distinct. If $z_j$ is a multiple zero instead, that is, $m_j \geq 2$, we can factor out $(z - z_j)^{m_j - 1}$ from (13), which yields

$$P'(z) = a_n(z - z_j)^{m_j - 1}Q(z), \tag{15}$$

where $Q(z)$ is a polynomial such that $Q(z_j) \neq 0$. Thus, it follows from (15) that $z_j$ is a zero of $P'(z)$ with multiplicity $m_j - 1$. □

Before we close this section, we remark that it can be shown that if the zeros of a polynomial $P$ lie on a line, then the zeros of $P'$ are more evenly spaced than the zeros of $P$. The aforementioned is also valid when $P$ is generalized to an entire function $f$ of order 1, and, given some stronger assumptions, when the zeros of $f$ lie in a suitable neighbourhood of a line or a circle. We state some of the aforementioned claims more formally in definitions 2.4-2.6 and Theorem 2.5 below.[3]

**Definition 2.4.** *A function $f : \mathbb{C} \to \mathbb{C}$ is said to be entire if it has a derivative at every point of $\mathbb{C}$.*

**Definition 2.5.** *The order $\rho$ of an entire function $f(z)$ is given by*

$$\rho = \limsup_{r\to\infty} \frac{\log\log M(r)}{\log r}, \tag{16}$$

*where $M(r) = \max_{|z|=r} |f(z)|$. That is, $f(z) = O(\exp(|z|^{\rho+\delta}))$ for all $\delta > 0$ and no $\delta < 0$.*

**Definition 2.6.** *Let $f$ be an entire function. The function $n(r)$ denotes the number of zeros of $f$ in $|z| \leq r$. If $f$ has only real zeros, then $n_+(r)$ (respectively $n_-(r)$) denote the number of zeros in $(0, r]$ (respectively, $[-r, 0)$).*

**Theorem 2.5.** *Suppose $f$ is an entire function of order 1 which is real on the real axis, has only real zeros, and $n_+(r) \sim n_-(r) \sim \kappa r$, for some $\kappa > 0$.*

*Then there exist sequences* $(A_n)$, $(B_n)$, *and* $(D_n)$ *with* $D_n$ *bounded, such that*

$$\lim_{n\to\infty} A_n e^{B_n z} f^{(n)}(\kappa^{-1} z + D_n) = \cos(\pi z), \tag{17}$$

*uniformly for* $|z| \leq X$ *for any fixed* $X > 0$. *In particular, the zeros of* $f^{(n)}$ *approach equal spacing.*

# 3 Geometrical changes of the zeros after successive differentiation

We are almost ready to begin our experimental investigations of how the zeros of a polynomial $P$ change after repeated differentiation. As previously stated, the focus will be on polynomials with simple zeros distributed in regular patterns in convex hulls. Unless otherwise stated, all zeros are illustrated with disks, and centers of mass (average values of the zeros) are represented by squares. Before we begin, however, we give the following four characteristics, which numerically describe different types of distance between the zeros.

**Definition 3.1.** *Let* $P$ *be a complex polynomial of degree* $n \geq 2$ *with the set* $\mathcal{Z}(P) = \{z_1, z_2, \ldots, z_n\}$ *of zeros. Then*

$$m(P) := \min\{|z_j - z_k| : z_j, z_k \in \mathcal{Z}(P), j \neq k\}, \tag{18}$$

$$M(P) := \max\{|z_j - z_k| : z_j, z_k \in \mathcal{Z}(P), j \neq k\}, \tag{19}$$

$$\widehat{m}(P) := \frac{1}{n}\sum_{j=1}^{n} \min\{|z_j - z_k| : z_k \in \mathcal{Z}(P), j \neq k\}, \tag{20}$$

*and*

$$\widehat{M}(P) := \frac{1}{n}\sum_{j=1}^{n} \max\{|z_j - z_k| : z_k \in \mathcal{Z}(P), j \neq k\}. \tag{21}$$

**Remark 3.1.** *As above,* $\mathcal{Z}(P)$ *denotes the set of zeros for a given polynomial* $P$.

**Example 3.1.** Consider the polynomial $P(z) = (z - 1 - \frac{5}{2}i)(z - 2 - i)(z - 3 - 2i)(z - 5 - \frac{3}{2}i)$ of degree 4 with zeros shown below in Figure 3.

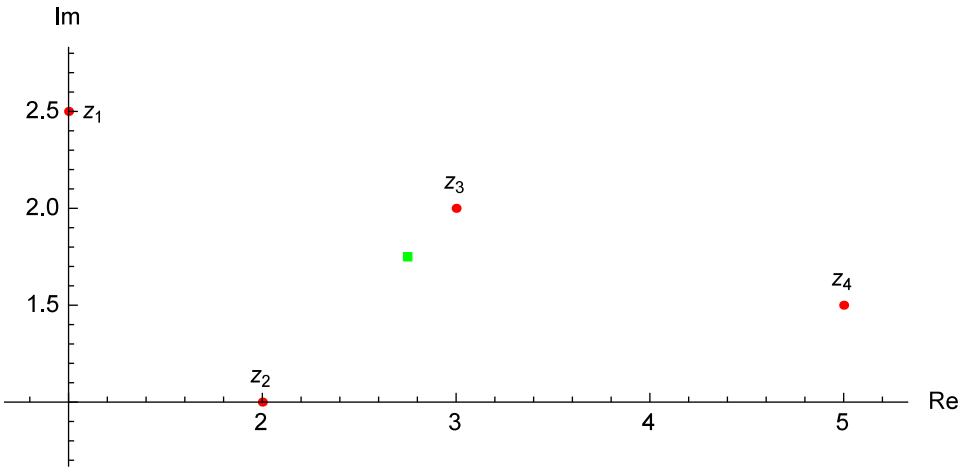


Figure 3: Four zeros of the polynomial $P(z)$. The square shows the average value of the zeros, $\frac{11}{4} + \frac{7}{4}i$.

The function $m(P)$ ($M(P)$) given in Definition 3.1 denotes the shortest (longest) distance between any pair of distinct zeros of $P(z)$. Similarly, $\widehat{m}(P)$ ($\widehat{M}(P)$) denotes the mean value of the distances between each zero and its nearest (most distant) neighbour.

It is easily seen in Figure 3 that $|z_1 - z_2| = \frac{\sqrt{13}}{2}$, $|z_1 - z_3| = \frac{\sqrt{17}}{2}$, $|z_1 - z_4| = \sqrt{17}$, $|z_2 - z_3| = \sqrt{2}$, $|z_2 - z_4| = \frac{\sqrt{37}}{2}$, and $|z_3 - z_4| = \frac{\sqrt{17}}{2}$. It follows that

$$m(P) = \sqrt{2} \approx 1.414, \tag{22}$$

$$M(P) = \sqrt{17} \approx 4.123, \tag{23}$$

$$\widehat{m}(P) = \frac{1}{4}\left(\frac{\sqrt{13}}{2} + \sqrt{2} + \sqrt{2} + \frac{\sqrt{17}}{2}\right) \approx 1.673, \tag{24}$$

and

$$\widehat{M}(P) = \frac{1}{4}\left(\sqrt{17} + \frac{\sqrt{37}}{2} + \frac{\sqrt{17}}{2} + \sqrt{17}\right) \approx 3.337. \tag{25}$$

We will carry out our investigations for different shapes that contain the zeros.

### 3.1 Triangles

Let $\mathcal{T}$ be the equilateral triangle in the first quadrant of the complex plane with side length $s \in \mathbb{N}$, such that the closed interval $[0, s]$ on the real axis is one of its sides. It is easily shown that $\mathcal{T}$ can be divided into $s^2$ non-overlapping, equilateral triangles, each with side 1. We define $p$ as the polynomial that has $(s+1)(s+2)/2$ simple zeros, each of which lies at the vertices of these non-overlapping triangles. Explicitly, $p$ is given by

$$p(z) := \prod_{m=0}^{s} \prod_{n=0}^{s-m} \left( z - \frac{1}{2}(m + 2n + \sqrt{3}mi) \right). \tag{26}$$

We illustrate the zeros of $p$ and some of its derivatives below in Figure 5, where we have chosen $s = 10$.

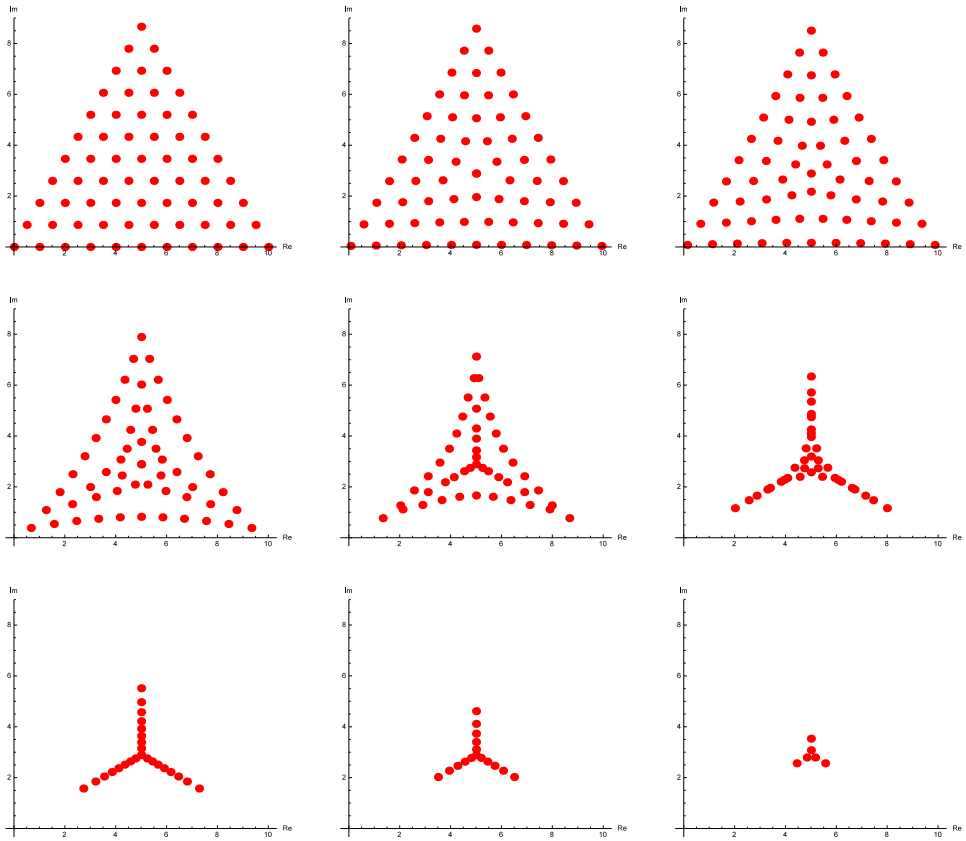

Figure 4: The zeros of $p$, $p'$, $p''$, $p^{(10)}$, $p^{(20)}$, $p^{(30)}$, $p^{(40)}$, $p^{(50)}$, and $p^{(60)}$, respectively, when $s = 10$. All zeros of $p^{(\ell)}$ lie on the three lines $re^{i\frac{\pi}{6}(4k+3)} + 5(1 + i/\sqrt{3})$ when $\ell \in \{34, 35, \ldots, 65\}$, where $r \geq 0$ and $k = 0, 1, 2$.

The zeros in Figure 4 behave similarly to point masses under the mutual influence of an attractive force that depends on distance. Furthermore, the

zeros are drawn toward their mutual center of mass, $5(1 + i/\sqrt{3})$. More specifically, the point masses in step $k$ give rise to a field of force, where the points of equilibrium lie in the positions of the zeros in step $k + 1$; see Theorem A.1 on page 69.

The functions $m(P), M(P), \widehat{m}(P)$, and $\widehat{M}(P)$, respectively, are shown below in Figure 5 for $p, p', \ldots, p^{(64)}$.

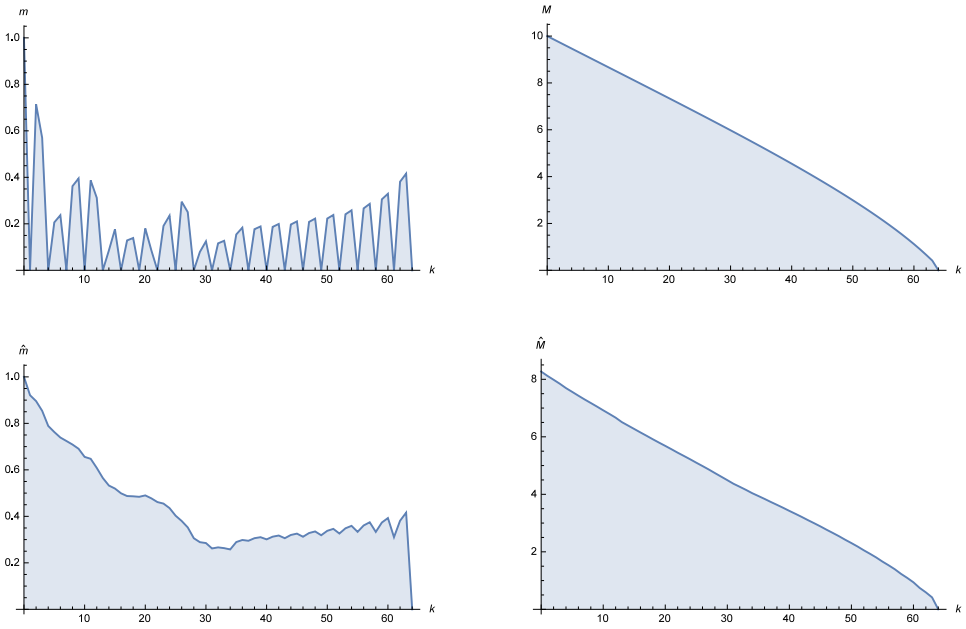


Figure 5: The value of $m(P)$, $M(P)$, $\widehat{m}(P)$ and $\widehat{M}(P)$, respectively, in the $k$:th derivative of polynomial $p$, when $s = 10$. Note that the given functions have discrete domains; thus the values for non-integer $k$ that are shown are irrelevant.

The periodic minimum of $m(P)$ in Figure 5 arises from a double root in the center of mass that appears every third differentiation (up until $k = 64$). Furthermore, the linearly decreasing appearance of $M(P)$ vanishes after $k = 34$ differentiations of $p$, and is replaced by an accelerating rate of decrease. This event coincides with the previously noted collapse of the zeros onto three lines with radial symmetry around the center of mass. Thus, the convex hull of the zeros shrinks at an even rate at first, then vanishes at an accelerating pace as soon as the last zeros have reached these lines. It is also noteworthy that this transition at $k = 34$ yields the global minimum of $\widehat{m}(P)$, if the final double root at $k = 64$ is omitted.

It should be noted that our choice to distribute the zeros of $p$ in the first quadrant is justified because the derivative is unaffected by some affine transformations of the $z$-plane, such as rotations, translations, and mirroring. For

instance, consider the situation that we translate the zeros of $p$ partially into the second quadrant by the vector $-7+2i$, then rotate them the angle $\pi/4$ counterclockwise around the origin, and let $q$ denote the polynomial with these new zeros. The zeros $\mathcal{Z}(q)$, $\mathcal{Z}(q^{(20)})$, and $\mathcal{Z}(q^{(30)})$ are shown below in Figure 6, where we see no difference from the shapes of $\mathcal{Z}(p)$, $\mathcal{Z}(p^{(20)})$, and $\mathcal{Z}(p^{(30)})$, respectively, in Figure 4.

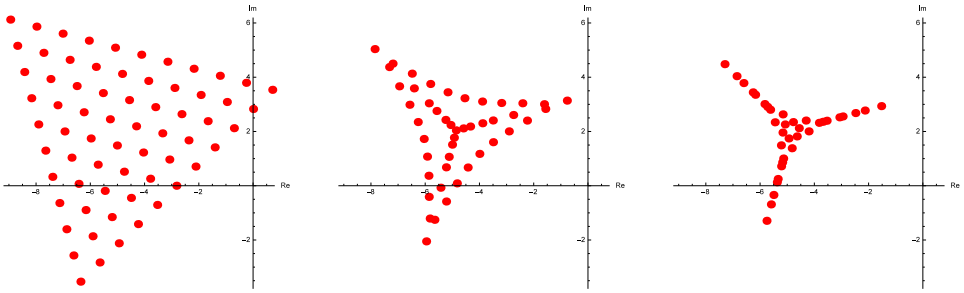

Figure 6: The zeros of $q$, $q^{(20)}$, and $q^{(30)}$.

To compress the definitions of certain types of polynomials that will be of interest to us, we introduce the following notation.

**Definition 3.2.** *Let $\mathcal{S}$ be a closed set, and let $\mathbf{Z}[i]$ be the Gaussian integers; that is, $\mathbf{Z}[i] := \{a+bi \mid a,b \in \mathbf{Z}\}$. Then $\mathcal{P}(\mathcal{S})$ is the polynomial with simple zeros of each point of the set $\mathbf{Z}[i] \cap \mathcal{S}$.*

**Remark 3.2.** *We will refer to $\mathcal{P}(\mathcal{S})$ as the lattice polynomial of $S$.*

To illustrate Definition 3.2, we let $\tilde{\mathcal{T}}$ be the isosceles triangle with its vertices in the complex numbers $\pm 15$ and $60i$, and define the polynomial $p := \mathcal{P}(\tilde{\mathcal{T}})$. The zeros of $p$ and some of its derivatives are shown below in Figure 7.

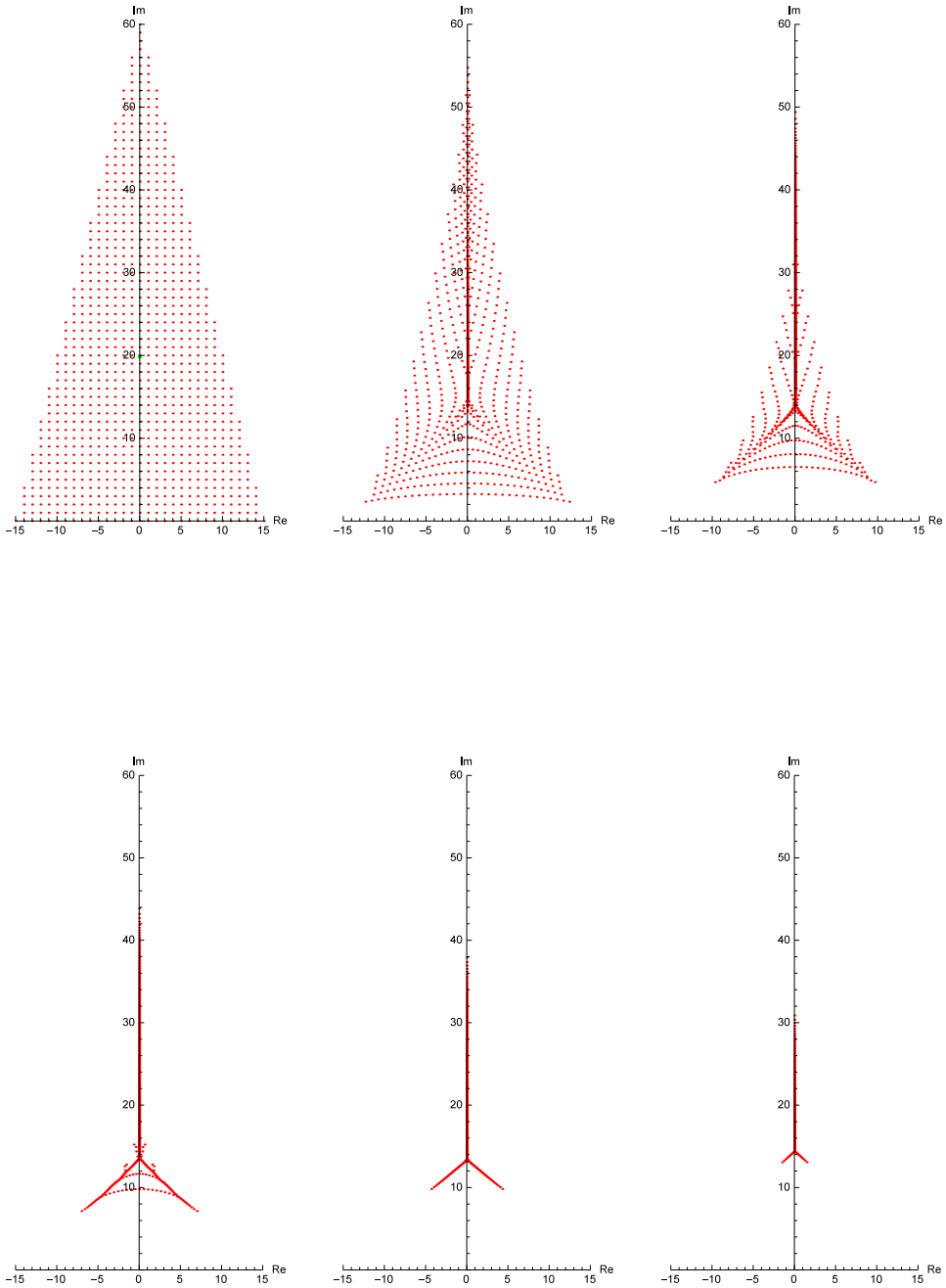


Figure 7: The zeros of $p$, $p^{(160)}$, $p^{(320)}$, $p^{(480)}$, $p^{(640)}$, and $p^{(800)}$, where $\deg(p) = 931$. The center of mass $m$ of the zeros is in each case $\frac{18490}{931}i \approx 19.86i$.

It is seen from Figure 7 that (analogously to the previous situation in Figure 4) the zeros of $p^{(700)}$ and $p^{(800)}$ are centered around three curves, which appear to be directed toward the vertices of $\tilde{\mathcal{T}}$ from a common point $w$. Unlike the previous case, however, $w$ is not the center of mass $m$ of the zeros of $p$, and furthermore, its position shifts gradually toward $m$. Upon closer inspection, two of the three 'branches' that emerge curve gently toward the real axis.

A strong clue about the position of $w$ in Figure 7 would emerge if the angles between adjacent pairs of curves, in some sense, are $120\,^\circ$. It turns out that any three distinct zeros of $p^{(800)}$, all of which have either nonpositive or nonnegative real parts, can be joined by two line segments such that no horizontal line intersects both of them, with a minimum angle $\alpha > 132.70\,^\circ$ between them. The analogous angle for the zeros of $p^{(640)}$ is $\beta > 127.38\,^\circ$, as long as only zeros from (one side of) the two-pronged fork structure are chosen. Clearly, the position of $w$ is affected by other factors. As we shall see later in section 3.5, $w$ seems to move in cycles with an overall drift toward the center of mass as the derivative is taken repeatedly.

Next, we generalize the triangle $\tilde{\mathcal{T}}$ by letting $\mathcal{T}(a)$ be the triangle with vertices in $\pm a$ and $4ai$ (so that $\mathcal{T}(a) = \tilde{\mathcal{T}}$ when $a = 15$), and consider what happens to the tree structure of the polynomial $q(a) := \mathcal{P}(\mathcal{T}(a))$ by increasing $a$ in steps. It can be shown with simple geometrical reasoning that $q(a)$ has $4a^2 + 2a + 1$ zeros. Consequently, we will try to replicate the tree of $p^{(800)}$ in Figure 7 by scaling the derivative to the number of zeros in $q(a)$. Because $p$ has 931 zeros, we will look at derivatives of order $\operatorname{nint}\left(\frac{800}{931}(4a^2 + 2a + 1)\right)$ for $q(a)$; see Figure 8 below.

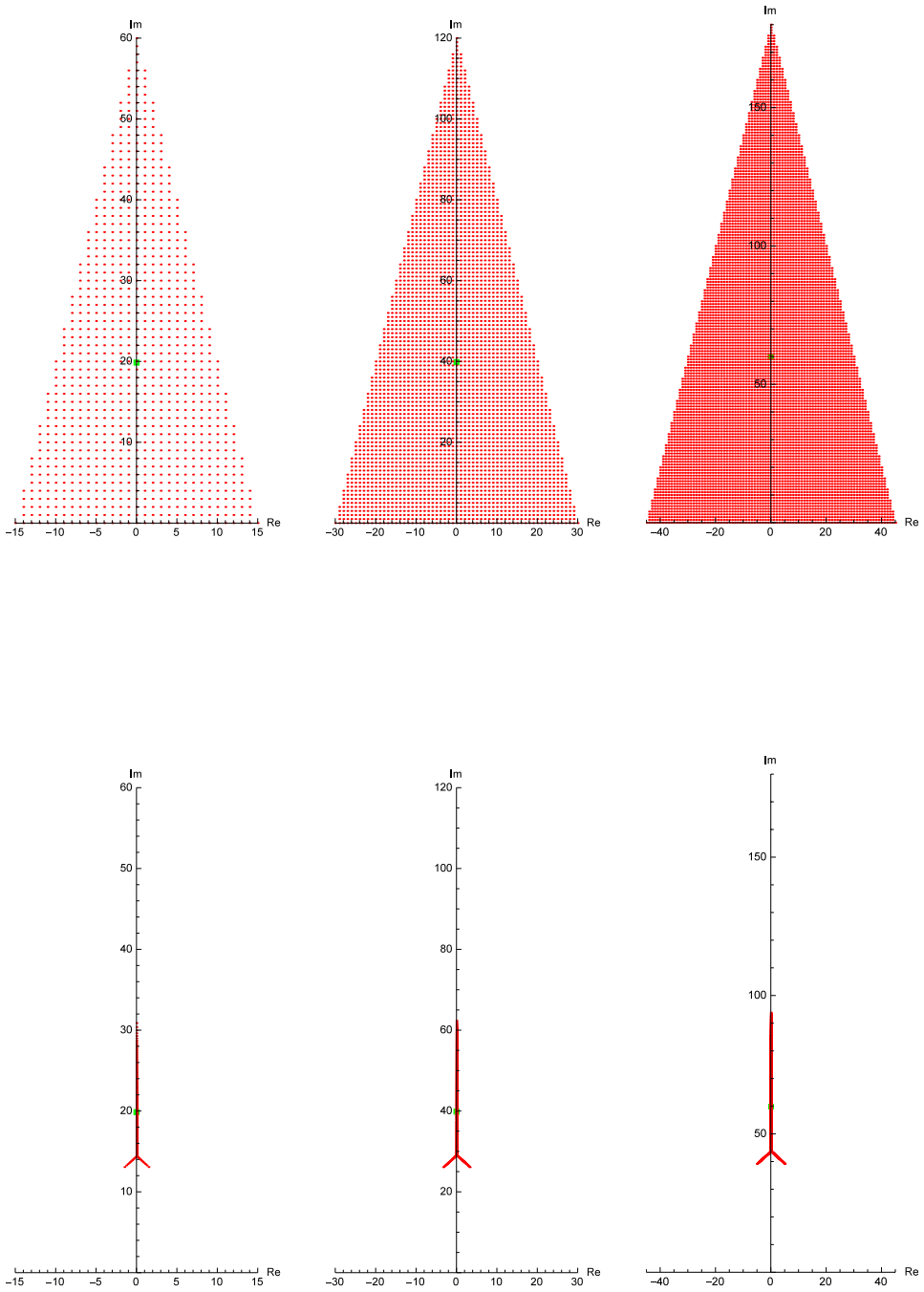


Figure 8: The zeros of $q(15)$, $q(30)$, and $q(45)$ (top row), and the zeros of their respective 800th, 3146th, and 7038th derivatives (bottom row).

It can be seen in Figure 8 that any two line segments formed by consecutive pairs of $180i$, the lowest zero of $q(45)$ on the real axis, and any zero of $q(45)$ with a positive real part have an angle $132.08\,^\circ < \alpha < 134.42\,^\circ$ between them. Thus, it is not clear that we have any significant convergence to $120\,^\circ$ angles between the three branches. Furthermore, it is clear from the figure that if $n$ denotes the degree of the polynomial $q(a)$ and $d$ is the order of the derivative, then fixing the quotient $n/d$ gives rise to almost identical tree structures. The only apparent difference (aside from the choice of scales) is the increased density of zeros for larger $n$. Furthermore, we have considered the zeros at the points $(n, d) = (931, 800), (3661, 3146), (8191, 7038)$ which (approximately) reside on a line in the $n - d$ plane. We will return to this plane shortly.

Next, we let $\widehat{\mathcal{T}}$ be the triangle with its vertices in the complex numbers $10, 30i$, and 60, and, as previously, define $p := \mathcal{P}(\widehat{\mathcal{T}})$; see Figure 9.

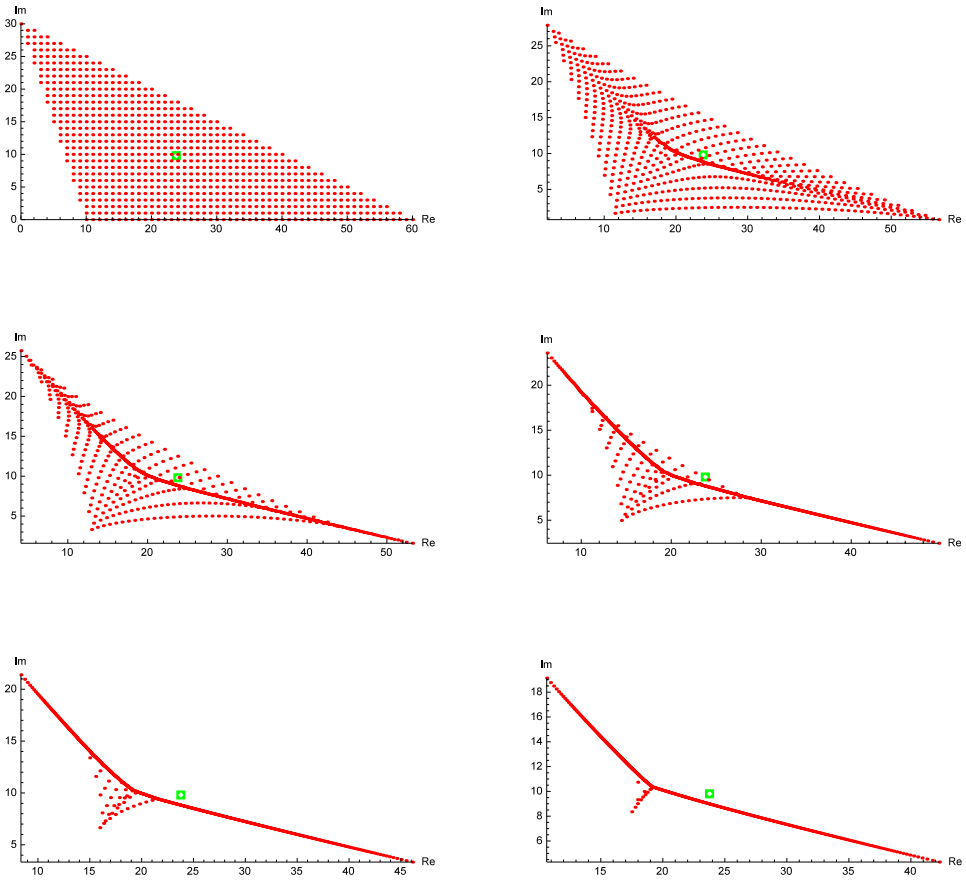

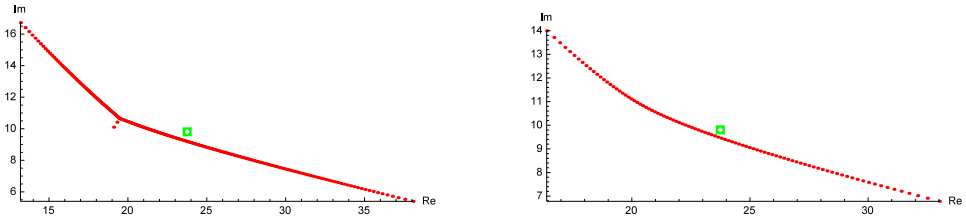


Figure 9: The zeros of $p$, $p^{(100)}$, $p^{(200)}$, $p^{(300)}$, $p^{(400)}$, $p^{(500)}$, $p^{(600)}$, and $p^{(700)}$, where $\deg(p) = 796$. The squares show the average values (or centers of mass) of the zeros. Note that the scales are automatically adjusted due to the relatively large size differences.

Similarly to the situation in Figure 7, Figure 9 shows that the zeros of $p^{(500)}$ and $p^{(600)}$ are apparently concentrated around three curves that branch off toward the vertices of $\widehat{\mathcal{T}}$ from a common point $w'$. Again, $w'$ gradually shifts toward the center of mass for higher derivatives.

Letting $q(n)$ denote a polynomial with $n$ simple zeros that have been Dirichlet distributed within $\widehat{\mathcal{T}}$, we repeat the experiment. The zeros of $q(796)$ and its 500th derivative are shown below in Figure 10.

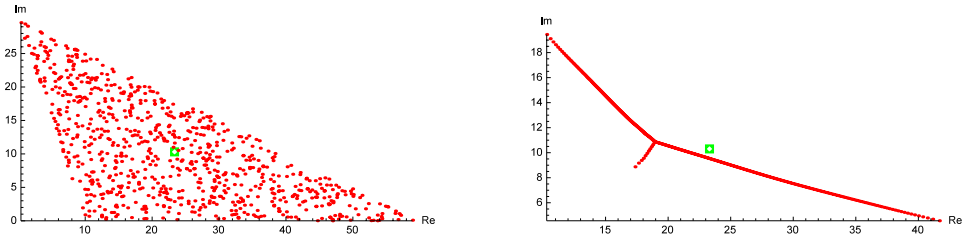


Figure 10: The zeros of $q(796)$ and $q(796)^{(500)}$.

By comparing the zeros of $q(796)^{(500)}$ in Figure 10 to the zeros of $p^{(500)}$ in Figure 9, it seems likely that the shapes of the three curves depends more on the shape of $\widehat{\mathcal{T}}$ than on the way in which the zeros are distributed inside $\widehat{\mathcal{T}}$. By the Gauss-Lucas theorem, however, it is clear that if all zeros of $q(n)$ end up being randomly distributed on a line, no such structure of three separate curves can arise in $q(n)^{(k)}$, $k = 1, \ldots, n$. In other words, the 'curve complex' of zeros cannot be completely independent of the way in which the zeros are distributed inside $\widehat{\mathcal{T}}$ in general.

Next, we show the zeros of $q(1592)$ and its 1000th derivative below in Figure 11.

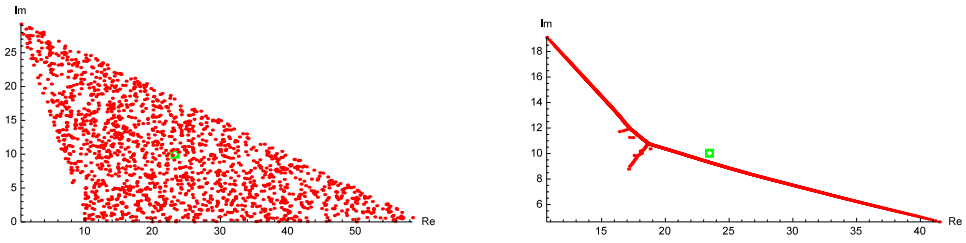


Figure 11: The zeros of $q(1592)$ and $q(1592)^{(1000)}$.

As previously seen in Figure 8, maintaining a fixed quotient $n/d$ ($n$ being the degree of the polynomial, $d$ being the order of the derivative) seems to stabilize the curves. In the cases of figures 10 and 11, $n/d = 796/500 = 1592/1000 = 1.592$, so we have considered the zeros at two points $(n, d) = (796, 500), (1592, 1000)$ along the line $L_1 : n = 1.592d$ in the $n - d$ plane, where we yet again see indications of stability for fixed $n/d$. We proceed by illustrating the behavior of the zeros of $q(n)$ (and of its derivatives) along the lines $L_2 : n = 2d$, $L_3 : n = (5/4)d$, and $L_4 : n = d + 100$ in this plane as well; see figures 12-14 below.

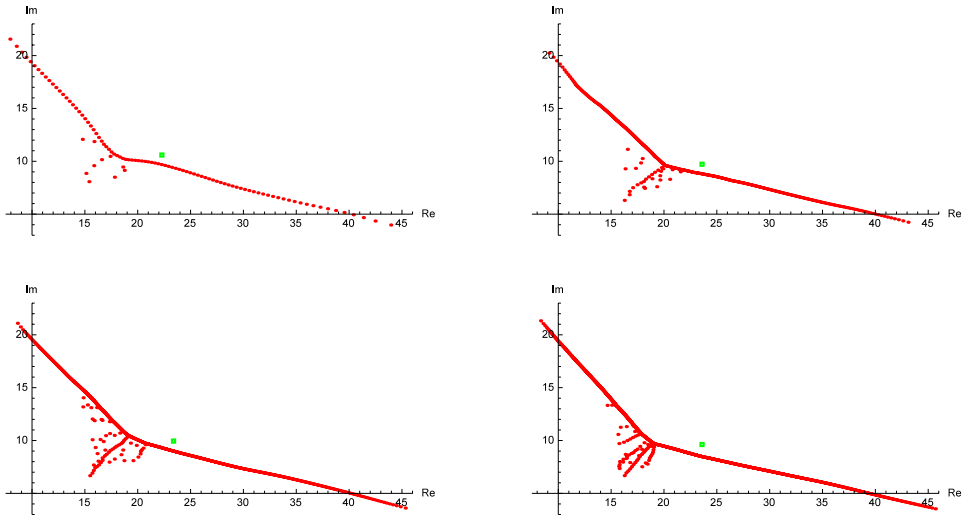


Figure 12: The zeros of $q(200)^{(100)}$, $q(600)^{(300)}$, $q(1000)^{(500)}$, and $q(1400)^{(700)}$ along the line $L_2 : n = 2d$.

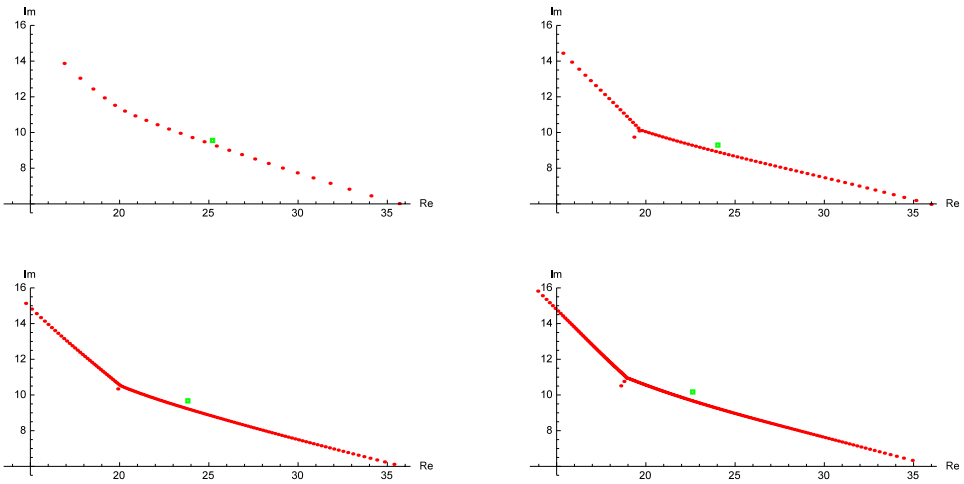


Figure 13: The zeros of $q(125)^{(100)}$, $q(375)^{(300)}$, $q(625)^{(500)}$, and $q(875)^{(700)}$ along the line $L_3 : n = (5/4)d$.

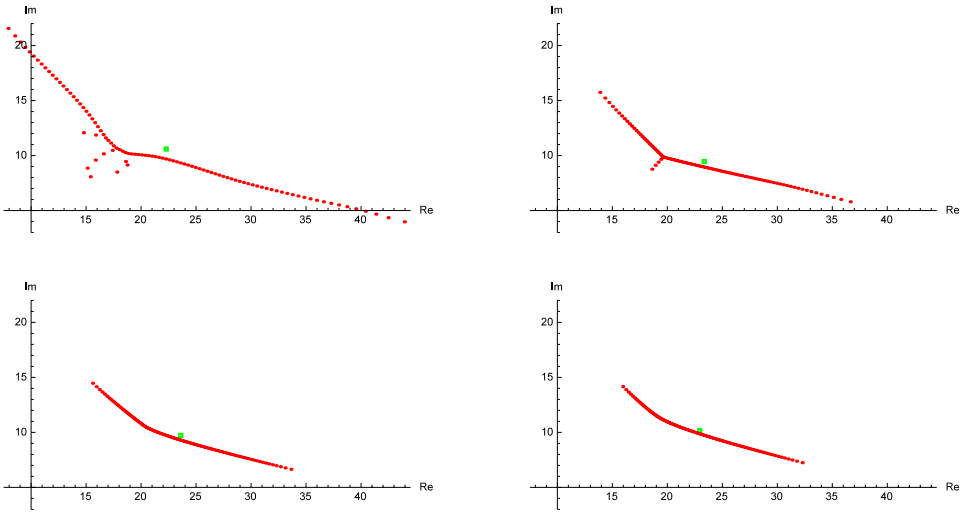


Figure 14: The zeros of $q(200)^{(100)}$, $q(400)^{(300)}$, $q(600)^{(500)}$, and $q(800)^{(700)}$ along the line $L_4 : n = d + 100$.

In Figure 12, we note that the trees stabilize for larger $n$, indicating again that a fixed $n/d$ quotient causes this behavior for growing $n$ and $d$. Furthermore, the successive straightening of the three branches shows that the effects of the random distribution of zeros decrease as more zeros are distributed. Similar behavior is shown in Figure 13, where the smaller (constant) ratio $n/d$ decreases the influence of the random distribution of zeros even more. It seems that zeros tend to be attracted toward the displayed tree structures (or their 'ideal' forms) when the derivative is taken many times relative to the size of $n$. Hints of evened out zero spacing is also shown along the branches. Finally, Figure 14 shows 100 zeros in each of the four cases, and we note that the resulting trees successively become smaller and more evolved. This follows because $n/d = (d+100)/d \to 1$ as $d \to \infty$, and whenever $n = d$, we get a maximally evolved structure (with no zeros left).

We conjecture that more interesting behaviors arise when points $(n, d)$ are considered along other curves in the $n - d$ plane, such as circles or circle segments. We will not investigate such geometries here.

The reader may have noticed that differentiating the polynomials above has left the centers of mass of their zeros unchanged. This is true in general for complex polynomials, as shown in the following, simple theorem.

**Theorem 3.1.** *Let $P(z) = a_n z^n + a_{n-1} z^{n-1} + \cdots + a_1 z + a_0$ be a polynomial of degree $n \geq 2$ with zeros $z_1, z_2, \ldots, z_n$ and critical points $\zeta_1, \zeta_2, \ldots, \zeta_{n-1}$. Then*

$$\frac{1}{n}\sum_{k=1}^{n} z_k = \frac{1}{n-1}\sum_{k=1}^{n-1} \zeta_k. \tag{27}$$

*Proof.* The fundamental theorem of algebra (Theorem A.2, page 69) lets us write $P(z)$ in the form

$$P(z) = a_n(z - z_1)(z - z_2)\cdots(z - z_n). \tag{28}$$

By multiplying the parentheses in equation (28) together, it is realized that the coefficient of $z^{n-1}$ is $-a_n(z_1 + z_2 + \cdots + z_n)$. Because this coefficient must be identical to the coefficient of $z^{n-1}$ in the original polynomial, it follows that

$$\sum_{k=1}^{n} z_k = -\frac{a_{n-1}}{a_n}. \tag{29}$$

Differentiating the original polynomial and using the same argument as for equation (29) shows that

$$\sum_{k=1}^{n-1} \zeta_k = -\frac{(n-1)a_{n-1}}{n a_n}. \tag{30}$$

By multiplying equation (30) with $n/(n-1)$ and comparing it to equation (29), the desired equality (27) follows. □

Before we proceed to quadrilaterals, we note that Theorem 3.1 can be generalized (asymptotically) to $k$:th moments of root measures as follows. (Some relevant measure-theoretic terminology is given in definitions A.1-A.4 on page 67.[10])

**Definition 3.3.** *Let $p$ be a polynomial of degree $n$, and construct a probability measure $\mu$ by placing a point mass of size $1/n$ at each zero of $p$. Then $\mu$ is called the root measure of $p$.*

**Definition 3.4.** *Let $p$ be a monic polynomial of degree $n \geq 1$ with root measure $\mu$. The logarithmic potential $u$ of $\mu$ is given by*

$$u(z) := \int \log|z-\zeta| \mathrm{d}\mu(\zeta) = \frac{1}{n}\log|p|. \tag{31}$$

*The Cauchy transform $C(z)$ of $\mu$ is given by*

$$C(z) := \int \frac{\mathrm{d}\mu(\zeta)}{z-\zeta} = \frac{p'(z)}{np(z)}. \tag{32}$$

**Theorem 3.2.** *Let $p_m$ be a sequence of polynomials, such that $n_m := \deg p_m \to \infty$ as $m \to \infty$, and let $\mu_m$ and $\mu'_m$ be the root measures of $p_m$ and $p'_m$, respectively. If $\mu_m \to \mu$ and $\mu'_m \to \mu'$ (weakly with compact support) and $u$ and $u'$ are the logarithmic potentials of $\mu$ and $\mu'$, then $u' \leq u$ with equality in the unbounded component of $\mathbb{C} \setminus \operatorname{supp}\mu$.*

We direct the interested reader to a paper by Tanja Bergkvist and Hans Rullgård for a proof of Theorem 3.2, which more generally deals with the zero distributions of eigenpolynomials of certain differential operators.[1]

Now, if $P_1$, $P_2$, ... is a sequence of monic polynomials of degrees 1, 2, ... that satisfies the assumptions in Theorem 3.2, then

$$\frac{1}{n}\log|P_n| \approx \frac{1}{n-1}\log\left|\frac{P'_n}{n}\right| \tag{33}$$

for all large enough $n$. This result can also be expressed in terms of the Cauchy transform $C_n(z)$ of the root measure $\mu_n$ of $P_n$,

$$\begin{aligned} u'(z) - u(z) &= \lim_{n\to\infty}\left(\frac{1}{n-1}\log\left|\frac{P'_n}{n}\right| - \frac{1}{n}\log|P_n|\right) = \lim_{n\to\infty}\frac{1}{n}\log\left|\frac{P'_n}{nP_n}\right| \\ &= \lim_{n\to\infty}\frac{1}{n}\log|C_n(z)|\,. \end{aligned} \tag{34}$$

From this, Bergkvist-Rullgård obtain the conclusions about $u$ and $u'$ in Theorem 3.2. A particular consequence is that the corresponding Cauchy transforms agree in a neighbourhood of infinity. This can be compared with our result Theorem 3.1, which expressed in terms of the Cauchy transforms, $C$ and $C'$, of the root measures for $P$ and $P'$ (respectively) says that

$$C(z) - C'(z) = O(|z|^{-2}) \quad \text{as } z \to \infty. \tag{35}$$

Note that each individual term is only $O(|z|^{-1})$ at infinity.

### 3.2 Quadrilaterals

Let $\mathcal{R}$ denote the rectangle in the complex plane with corners in the points $a+ci$, $a+di$, $b+ci$, and $b+di$, where $a, b, c$, and $d$ are positive integers such that $a < b$, $c < d$. Furthermore, let $p$ be the polynomial with simple zeros in the Gaussian integers in $\mathcal{R}$; that is, $p := \mathcal{P}(\mathcal{R})$. More explicitly, $p$ is the polynomial

$$p(z) := \prod_{m=a}^{b} \prod_{n=c}^{d} (z - (m + ni)) \tag{36}$$

of degree $(b-a+1)(d-c+1)$. We illustrate the zeros of $p$ and some of its derivatives below in Figure 15, when $-a = b = 8$ and $-c = d = 1$. Furthermore, Figure 16 shows the values of the functions $m(P)$, $M(P)$, $\widehat{m}(P)$, and $\widehat{M}(P)$, respectively, for $p$, $p'$, $\ldots$, $p^{(49)}$.

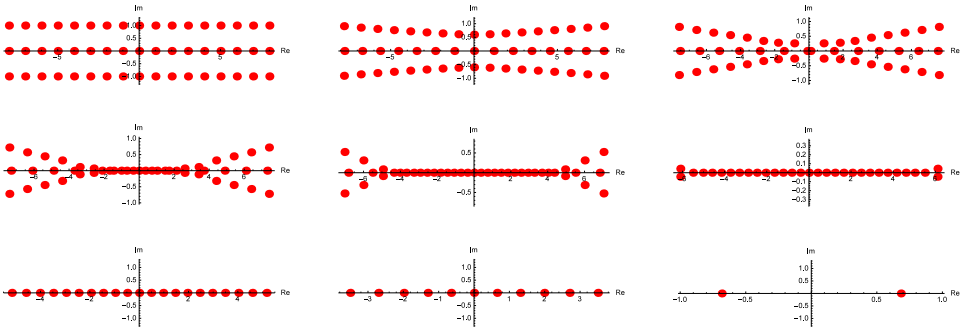

Figure 15: The zeros of $p, p'', p^{(4)}, p^{(6)}, p^{(10)}, p^{(20)}, p^{(30)}$, $p^{(40)}$, and $p^{(49)}$, respectively, when $a = -8$, $b = 8$, $c = -1$, and $d = 1$.

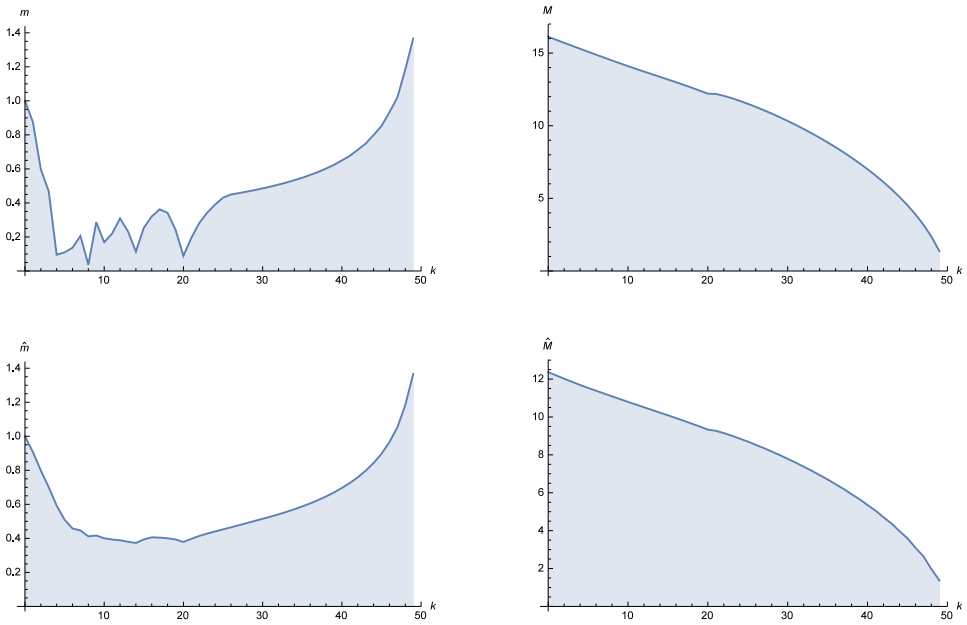


Figure 16: The value of $m(P)$, $M(P)$, $\widehat{m}(P)$, and $\widehat{M}(P)$, respectively, in the $k$'th derivative of the polynomial $p$, when $a = -8$, $b = 8$, $c = -1$, and $d = 1$.

The linearly decreasing appearance of $M(P)$ in Figure 16 disappears after $k = 20$ differentiations of $p$. In particular, the zeros of $p^{(k)}$ lie on the real axis for $21 \leq k \leq 50$ (see Figure 15), where $M(P)$ decreases more rapidly. This increased contraction speed of the convex hull of the zeros is analogous to the one seen for the polynomial in figure 4 on page 13; however, the convex hull has zero area in this case.

It is also seen in Figure 16 that the functions $m(P)$ and $\widehat{m}(P)$ have their maxima at $k = 49$. In particular, $1 < m(p^{(47)}) < m(p^{(48)}) < m(p^{(49)}) = 2\sqrt{7/15}$, so the separation of zeros becomes larger than the initial one for $p$, despite the shrinking of the convex hull. In fact, this largest minimum separation between zeros of $p^{(k)}$, $k = 1, 2, \ldots$ can be made arbitrarily large by increasing the width of $\mathcal{R}$, as in Figure 17.

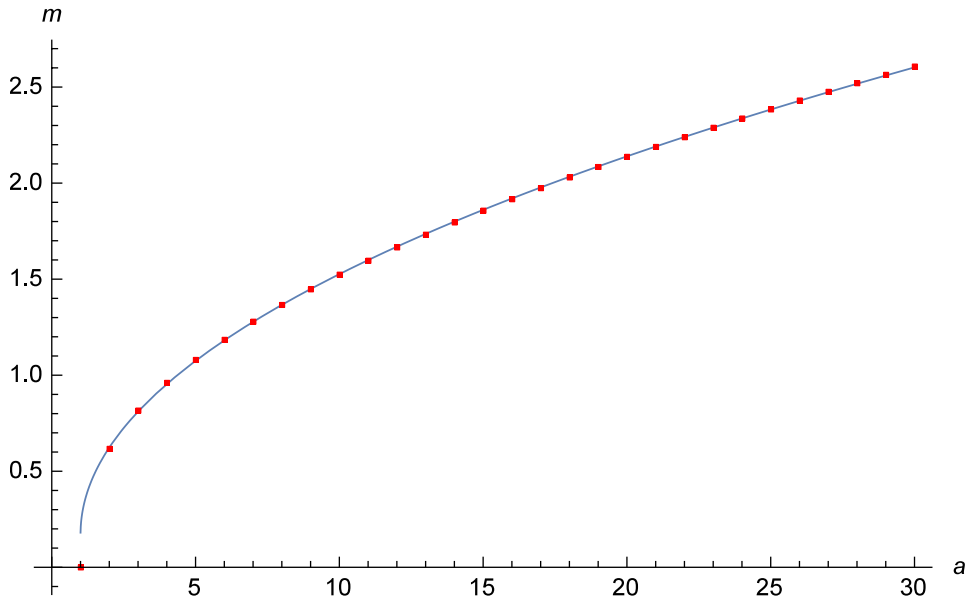


Figure 17: Distance between the last two zeros after $6a+1$ differentiations of $p(z) = \prod_{m=-a}^{a} \prod_{n=-1}^{1} (z-(m+ni))$, for $a = 1, 2, \ldots, 30$. The curve shown is given by $y = 0.45128\sqrt{a-1} + 0.17221$.

Curiously, no function of the form $y(a) = c_1\sqrt{a+c_2} + c_3$, where $c_1$, $c_2$, and $c_3$ are real constants, fits any four points in Figure 17 exactly.

Continuing with more general quadrilaterals, we let $Q$ be the simple 4-gon with corners in 0, $10+40i$, $40+35i$, and 60, and let $p := \mathcal{P}(Q)$. As before, we illustrate the zeros of the polynomial $p$ and some of its derivatives below in Figure 18.

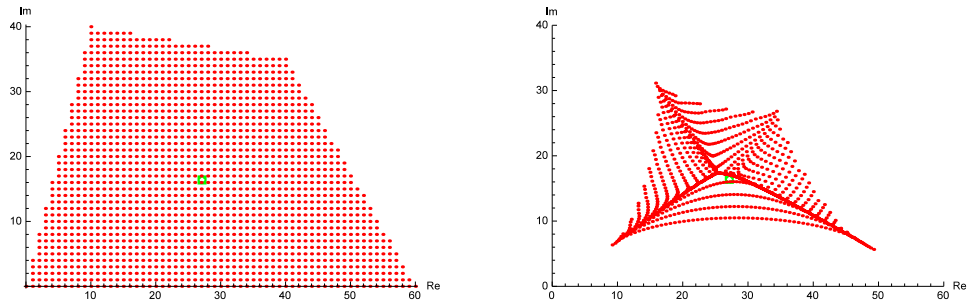

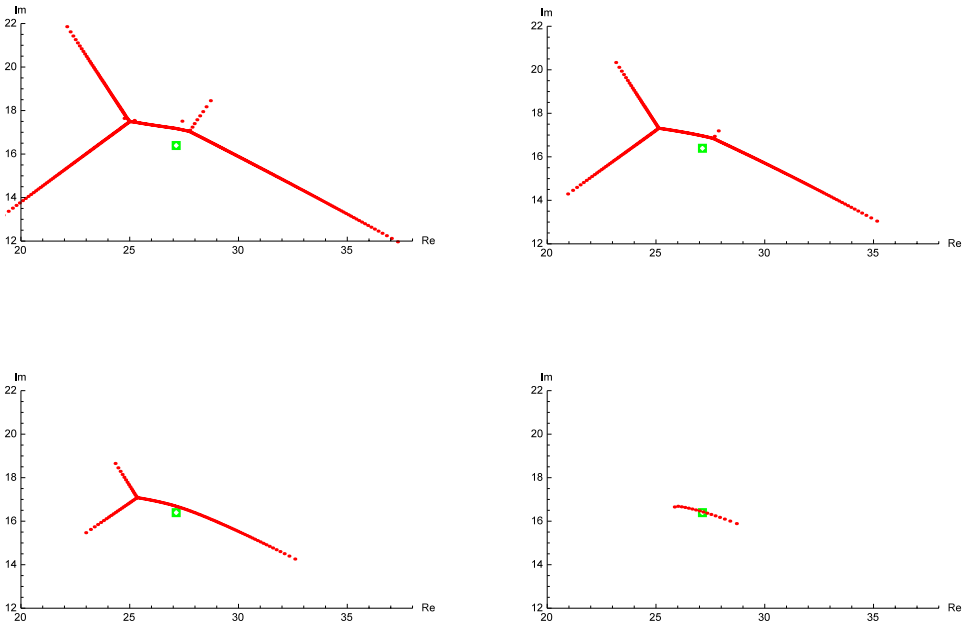


Figure 18: The zeros of $p$, $p^{(700)}$, $p^{(1400)}$, $p^{(1500)}$, $p^{(1600)}$, and $p^{(1700)}$, where $\deg(p) = 1716$.

Similarly to many of the polynomials in section 3.1, we evidently see tree structures in Figure 18, which contain up to four curves that branch off toward the vertices of $Q$ from a common 'trunk'. Furthermore, the spacing of the zeros appears to equalize from $p^{(1600)}$ to $p^{(1700)}$, analogously to the situation in Theorem 2.5 on page 10 where the zeros are distributed on lines. Based on these observations, and on the previous observations for figures 7-10, we give the following definitions and conjectures, some of which are inspired by graph theory (see definitions A.5-A.13 on pages 68-69[4]).

**Definition 3.5.** *A warped curve is a smooth curve $\mathcal{C}$ in the complex plane. If $\mathcal{C}$ can be intersected by a line in at most two points and contains no line segments, or is a line (segment), it is said to be strict.*

**Definition 3.6.** *Let $T = (V, E)$ be a tree. An edge $e \in E$ is called a twig if exactly one of its two vertices is a leaf vertex.*

**Definition 3.7.** *A warped tree is a planar embedding of a tree $T = (V, E)$, such that each edge $e \in E$ is a warped curve. If all of its warped curves are strict, then the warped tree itself is strict.*

**Definition 3.8.** *A warped forest is a planar embedding of a forest $F = (V, E)$, such that each edge $e \in E$ is a warped curve. If all of its warped curves are strict, then the warped forest itself is strict.*

**Conjecture 3.1.** *Let $P$ be a polynomial of degree $n \geq 3$ with its zeros on*

*a warped curve. Then the zeros of $P^{(k)}$ lie on a warped curve $H(k)$ and approach equal spacing.*

**Conjecture 3.2.** *Let $P$ be a polynomial of degree $n \geq 2$, and let $\widehat{H}$ be the set of all strict warped trees that each contain its $n$ zeros. Furthermore, let $H \in \widehat{H}$ have the smallest number $m$ of edges (warped curves). Then the zeros of $P'$ lie on a strict warped tree with at most $m$ edges.*

Analogously to the situation in Figure 10 on page 20, we continue by letting $q$ be a polynomial with Dirichlet distributed simple zeros inside $Q$, such that $\deg(q) = \deg(p) = 1716$; see Figure 19 below.

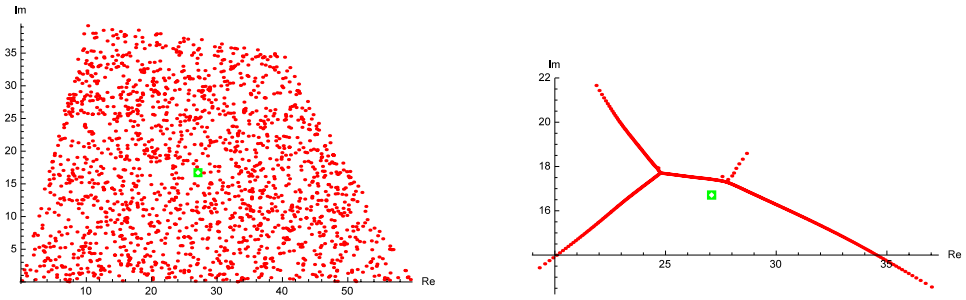


Figure 19: The zeros of $q$ and $q^{(1400)}$.

We note that the tree structures of the zeros of $p^{(1400)}$ in Figure 18 and $q^{(1400)}$ in Figure 19 have very similar shapes and sizes. Thus, we (again) conjecture that the tree structure that emerges is largely independent of how the zeros are 'evenly' distributed within shapes $\mathcal{S}$.

Because the four vertices of $Q$ can be connected with four line segments to form two separate polygons $Q_1$ and $Q_2$ that are not simple, we define $p_1 := \mathcal{P}(Q_1)$ and $p_2 := \mathcal{P}(Q_2)$; see Figure 20 below.

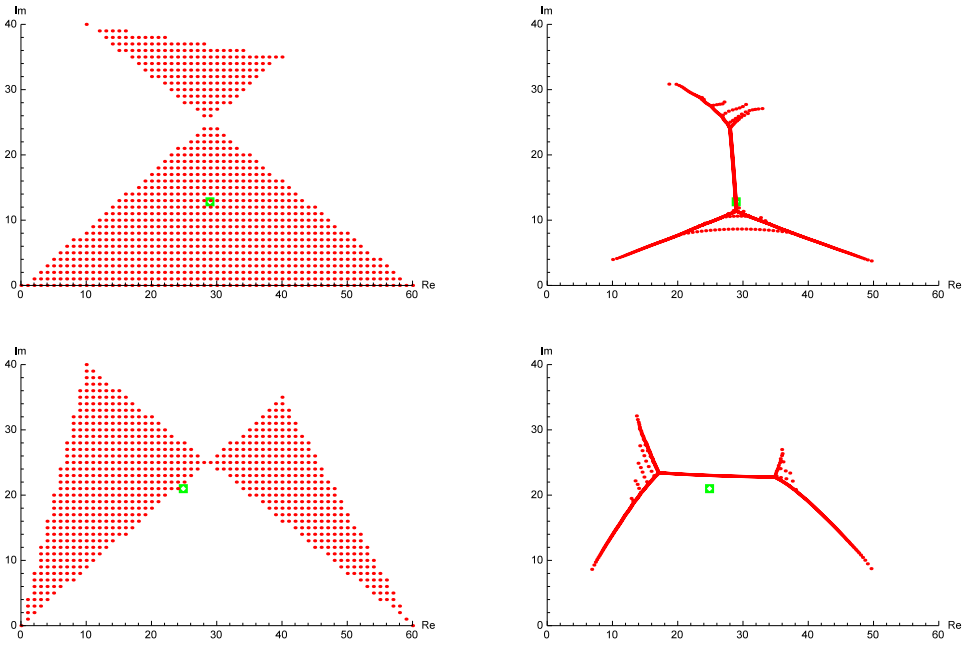


Figure 20: The zeros of $p_1$ and $p_2$ (left column), and the zeros of $p_1^{(395)}$ and $p_2^{(312)}$ (right column). In each case, the order $d$ of the derivative has been chosen so that $n/d \approx 700/1716$, where $n$ is the degree of the polynomial under consideration.

Even though $\deg(p_2) = 764 < 969 = \deg(p_1)$, the horizontal branch for $p_2$ is longer than the vertical branch for $p_1$ in Figure 20 by $\sim 5.0 - 5.5$ length units. This dominance of the horizontal branch is most likely related to the existence of the horizontal branch in Figure 18, whose length is $\sim 2.8$ units in $p^{(1400)}$, and $\sim 2.6$ units $p^{(1500)}$. It would hardly be a surprise if the horizontal branch length of $p^{(700)}$ turns out to be $\sim 5$ units in length, but it is difficult to tell from the figure alone.

Next, we double the side lengths of $Q$. Let $\tilde{Q}$ denote the resulting shape, and define $\tilde{p} = \mathcal{P}(\tilde{Q})$, which is a polynomial of degree 6781. Furthermore, we let $\hat{p}$ be a polynomial with a threefold increase in zeros from $p$, where the zeros have successively been scaled down toward the center of mass twice. The three layers of zeros of $\hat{p}$ (none of which have any overlapping zeros) have widths 60, 40, and 20, respectively; see figures 21-23.

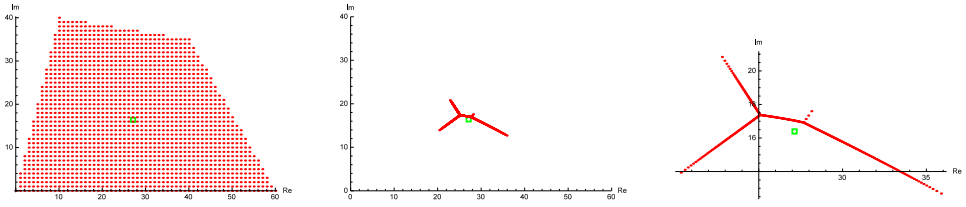

Figure 21: The zeros of $p$, $p^{(1468)}$ (fixed axes), and $p^{(1468)}$ (scaled axes), where $\deg(p) = 1716$.

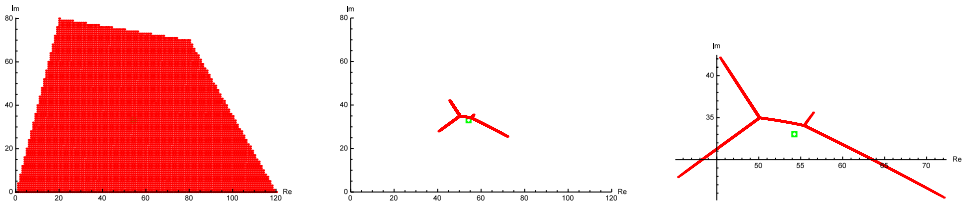

Figure 22: The zeros of $\tilde{p}$, $\tilde{p}^{(5801)}$ (fixed axes), and $\tilde{p}^{(5801)}$ (scaled axes), where $\deg(\tilde{p}) = 6781$.

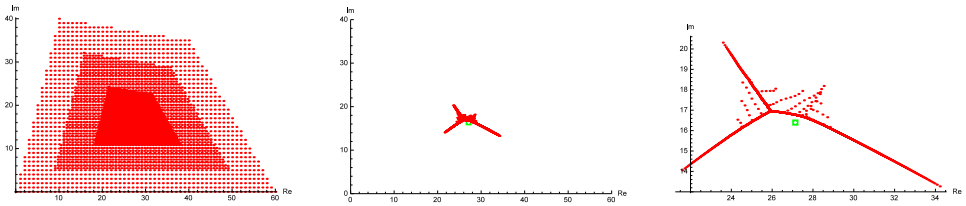

Figure 23: The zeros of $\hat{p}$, $\hat{p}^{(4404)}$ (fixed axes), and $\hat{p}^{(4404)}$ (scaled axes), where $\deg(\hat{p}) = 5148$.

In each case in figures 21-23, the order $d$ of the derivative has been chosen so that the quotient $n/d$ remains approximately constant, where $n$ is the

degree of the polynomial. Not surprisingly, the trees in figures 21 and 22 are almost identical, with the exceptions of their scales, and the tree for the latter has a higher density of zeros. The tree in Figure 23 shares similarities with the two previous trees discussed, but is notably smaller than the tree for $p$ (despite the convex hulls of $\mathcal{Z}(p)$ and $\mathcal{Z}(\hat{p})$ being identical) and has less evolved branches.

Inspired by the aforementioned differences between the trees for $p$ and $\hat{p}$, we try to scale up the tree by focusing zeros along the boundary of $Q$. Specifically, let $\widetilde{p}$ be the polynomial of degree 1716 with one zero in each corner of $Q$, each being of multiplicity $1716/4 = 429$. In other words,

$$\widetilde{p} := (z(z-(10+40i))(z-(40+35i))(z-60))^{429}. \tag{37}$$

As usual, we illustrate the zeros of $\widetilde{p}$ and some of its derivatives below in Figure 24.

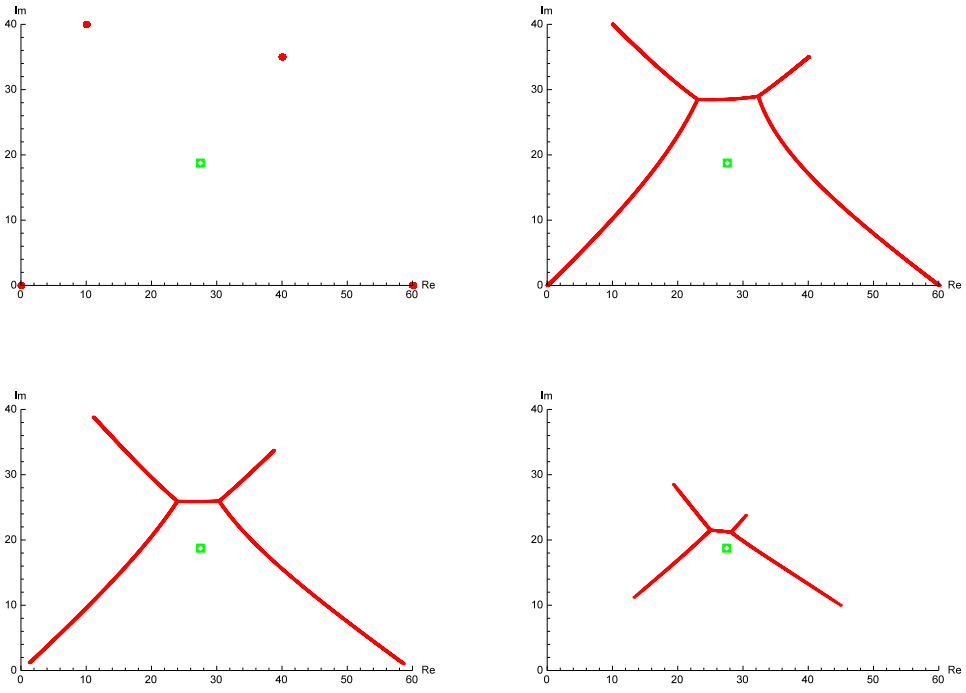


Figure 24: The zeros of $\widetilde{p}$, $\widetilde{p}^{(429)}$, $\widetilde{p}^{(700)}$ and $\widetilde{p}^{(1400)}$.

By the Gauss-Lucas theorem, and Theorem 2.4 on page 9, we note in Figure 24 that $d = 429$ is the smallest value of $d$ such that $\widetilde{p}^{(d)}$ has no zeros in the vertices of $Q$. Because of the apparent well-behaved nature of this tree structure, and its similarity to the previous trees generated from polynomials associated with $Q$, we investigate an analogous polynomial $\widetilde{P}(k)$ for the rectangle $\mathcal{R}$ at the start of this section. That is, we let

$$\widetilde{P}(k) := ((z-(-8-i))(z-(-8+i))(z-(8-i))(z-(8+i)))^k, \tag{38}$$

where $k \in \mathbb{N}$. We consider the cases $k = 100$ and $k = 300$ below in figures 25 and 26, respectively.


Figure 25: The zeros of $\widetilde{P}(100)$ and its 100th derivative, where $\deg\left(\widetilde{P}(100)\right) = 400$.


Figure 26: The zeros of $\widetilde{P}(300)$ and its 300th derivative, where $\deg\left(\widetilde{P}(300)\right) = 1200$.

Unfortunately, as we see in figures 25 and 26, it is not clear whether the three curve segments will grow arbitrarily close for larger $k$. Even in the event that the segments are disconnected, they appear fairly well-behaved, and we offer the following three definitions and two conjectures to aid us in their identification.

**Definition 3.9.** *Let $\mathcal{S}$ be a polygon with distinct vertices $z_1, \ldots, z_m$, and let $k \in \mathbb{N}$. Then $\mathcal{V}(\mathcal{S}, k)$ is the polynomial with a zero of multiplicity $k$ in each of the $m$ vertices of $\mathcal{S}$; that is,*

$$\mathcal{V}(\mathcal{S}, k) := \prod_{j=1}^{m} (z - z_j)^k. \tag{39}$$

**Definition 3.10.** *Let $\mathcal{S}$ be a polygon with distinct vertices $z_1, z_2, \ldots, z_m$, and let $P := \mathcal{V}(\mathcal{S}, k)$ for some $k \in \mathbb{N}$. The iterated forest of $\mathcal{S}$ of order $k$, denoted $\mathcal{F}(\mathcal{S}, k)$, is the set of zeros of $P^{(k)}$, that is,*

$$\mathcal{F}(\mathcal{S}, k) := \mathcal{Z}(P^{(k)}). \tag{40}$$

**Remark 3.3.** *If $p := \mathcal{V}(\mathcal{S}, 1)$, then $\mathcal{F}(\mathcal{S}, k)$ is the set of zeros of $(p^k)^{(k)}$.*

Note in Definition 3.10 that if we let $n$ denote the degree of the polynomial $P := \mathcal{V}(\mathcal{S}, k)$, then the order of the derivative $d = k$ yields that $n/d = mk/k = m$. We remind the reader that we have previously seen (in figures 8, 21, and 22, for example) that if we let $n$ and $d$ increase so that the quotient $n/d$ remains fixed, the resulting tree structures tend to stabilize and become saturated with zeros. Due to this behavior, we give the following definition of an iterated forest with the maximum saturation of zeros.

**Definition 3.11.** *Let $\mathcal{S}$ be a polygon with distinct vertices $z_1, z_2, \ldots, z_m$. The intrinsic forest of $\mathcal{S}$, denoted $\mathcal{F}(\mathcal{S})$, is given by*

$$\mathcal{F}(\mathcal{S}) := \lim_{k\to\infty} \mathcal{F}(\mathcal{S}, k) = \lim_{k\to\infty} \mathcal{Z}(\mathcal{V}(\mathcal{S}, k)^{(k)}). \tag{41}$$

At this point, we haven't shown the conditions under which the limit in equation (41) exists, nor what it converges to. We offer the following conjecture for intrinsic forests based on warped forests (see Definition 3.8, page 28).

**Conjecture 3.3.** *Let $\mathcal{S}$ be a polygon with distinct vertices $z_1, z_2, \ldots, z_m$. Then the intrinsic forest $\mathcal{F}(\mathcal{S})$ exists, and is a warped forest. Furthermore, $\mathcal{F}(\mathcal{S}) \neq \mathcal{F}(\mathcal{Q})$ for any polygon $\mathcal{Q} \neq \mathcal{S}$.*

While the definition of warped forests and the convergence criteria for Conjecture 3.3 might require some refinement, we note that if the conjecture is valid, we can approximate the unique warped forests associated with arbitrary polygons $\mathcal{S}$ to any desired degree of accuracy by using iterated forests. It might also be the case that all intrinsic forests are actually warped trees.

Since we haven't illustrated any iterated forests for the triangular polygons in section 3.1, we take the opportunity to do so now in figures 27-30 below.

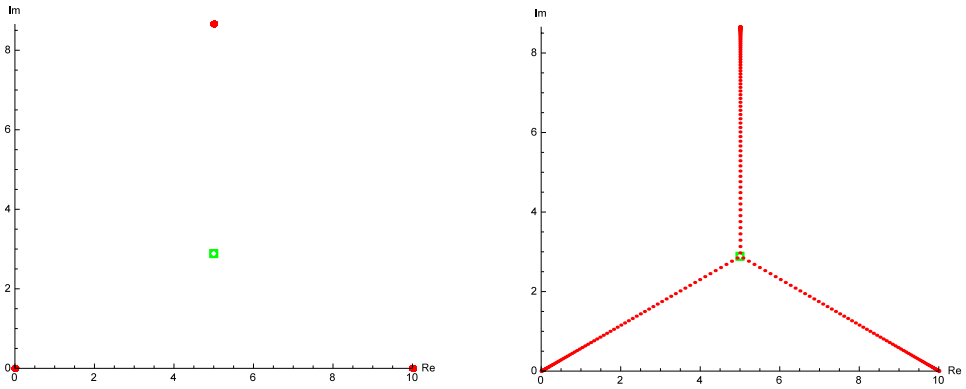


Figure 27: The zeros of $\mathcal{V}(\mathcal{T}, 100)$, and the iterated forest $\mathcal{F}(\mathcal{T}, 100)$.

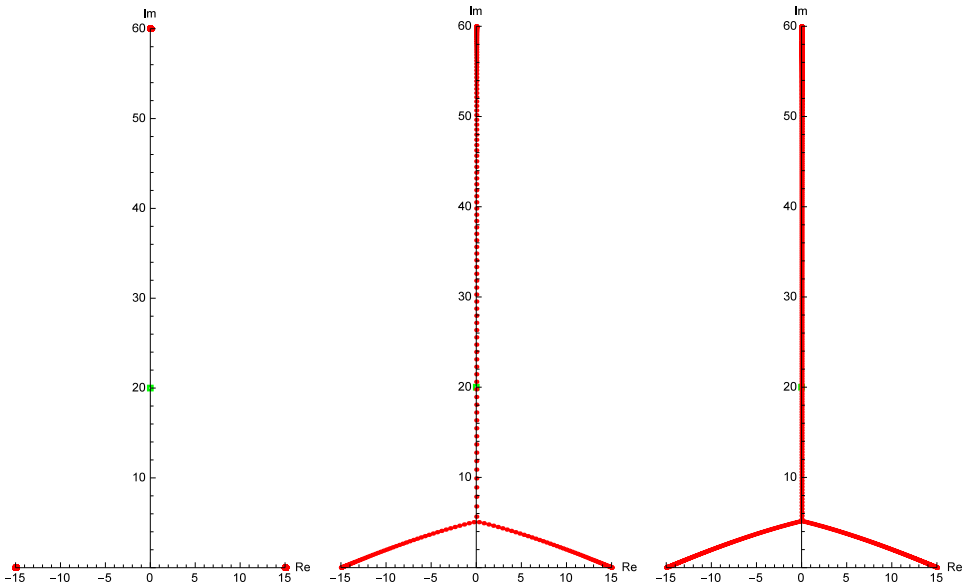


Figure 28: The zeros of $\mathcal{V}(\tilde{\mathcal{T}}, 100)$, and the iterated forests $\mathcal{F}(\tilde{\mathcal{T}}, 100)$ and $\mathcal{F}(\tilde{\mathcal{T}}, 300)$.

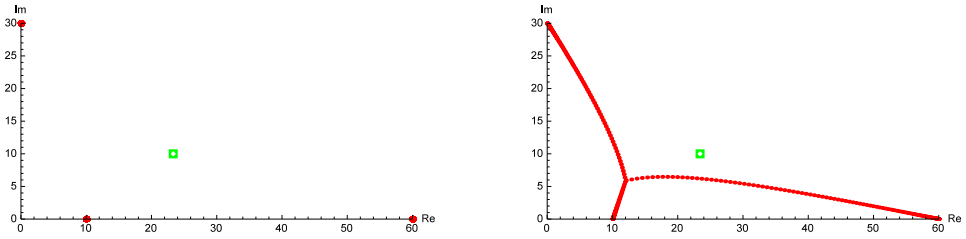


Figure 29: The zeros of $\mathcal{V}(\widehat{\mathcal{T}}, 100)$, and the iterated forest $\mathcal{F}(\widehat{\mathcal{T}}, 100)$.

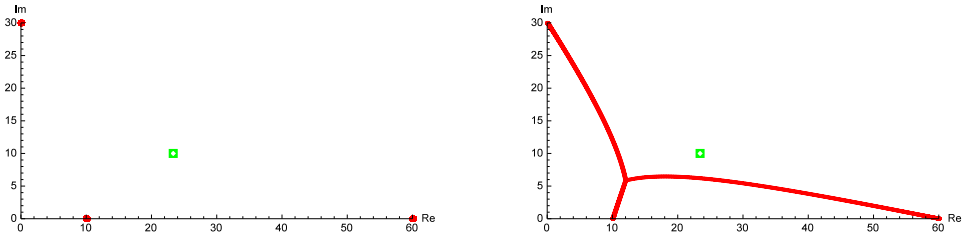


Figure 30: The zeros of $\mathcal{V}(\widehat{\mathcal{T}}, 300)$, and the iterated forest $\mathcal{F}(\widehat{\mathcal{T}}, 300)$.

As figures 27-30 indicate, it can generally be made obvious with an illustration of the iterated forest $\mathcal{F}(\mathcal{S}, k)$ what its defining polynomial $\mathcal{V}(\mathcal{S}, k)$ is. Hence, we will not bother to illustrate the zeros for the latter from now on. We may, however, choose to illustrate the associated polygon $\mathcal{S}$ with dashed lines to indicate more clearly how the iterated, and possibly intrinsic, forests relate to $\mathcal{S}$.

Next, we let $\mathcal{Q}_1$ be the concave quadrilateral whose edges are consecutive pairs of the vertices 0, $30+8i$, $40+35i$, 60, and 0, and let $p := \mathcal{P}(\mathcal{Q}_1)$. The situation is shown below in Figure 31.

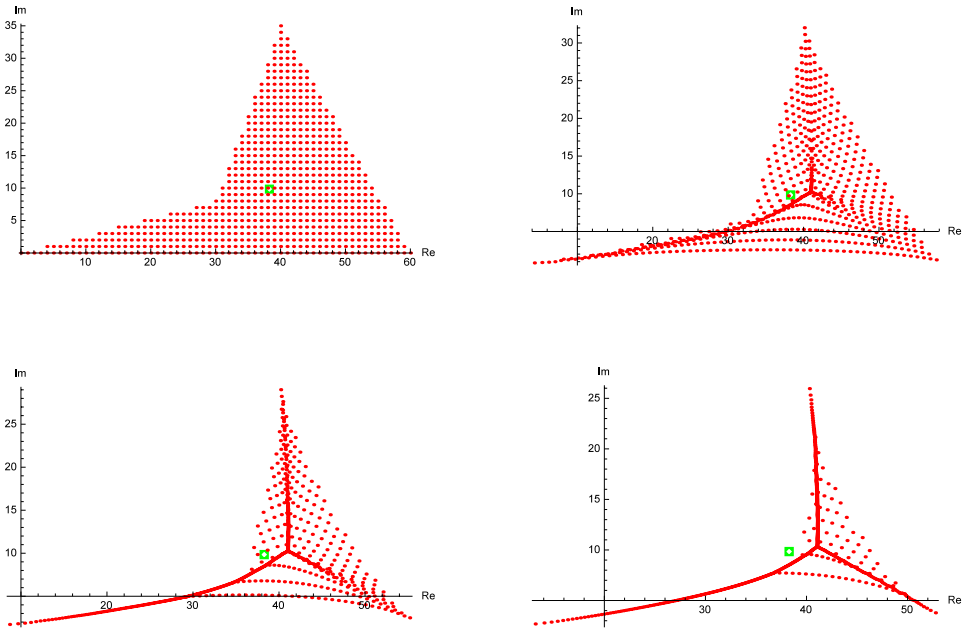

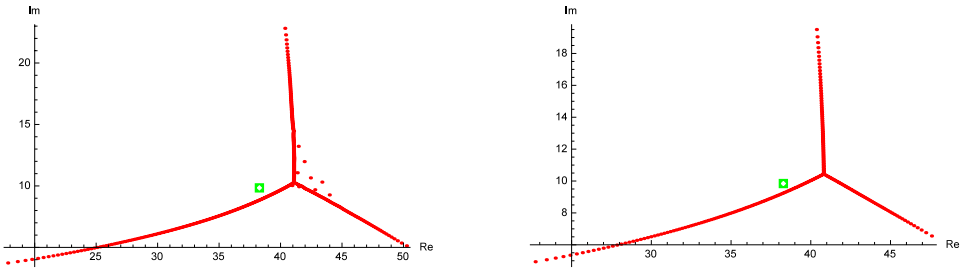


Figure 31: The zeros of $p$, $p^{(100)}$, $p^{(200)}$, $p^{(300)}$, $p^{(400)}$, and $p^{(500)}$, where $\deg(p) = 720$.

Apparently, the zeros of $p^{(k)}$ in Figure 31 coalesce around a tree structure similar to the one in Figure 18, but this time, we see three branches rather than four. It seems that the convex hull of the shape $\mathcal{Q}_1$, rather than $\mathcal{Q}_1$ itself, controls the structure of this tree. Based on this observation, we state the following conjecture.

**Conjecture 3.4.** *Let $\mathcal{G}_w$ be a simple polygon in the complex plane with positive area and width $w$, with the property that $\mathcal{G}_w$ shrinks (grows) linearly to (from) some point $p_0$ without otherwise deforming when $w \to 0$ ($w \to \infty$). Furthermore, let $\mathcal{S}_w$ be the closed set consisting of the points in $\mathcal{G}_w$. Then there exist constants $\lambda \in \mathbb{R}^+$ and $k \in \mathbb{N}$ such that the zeros of the $k$:th derivative of $\mathcal{P}(\mathcal{S}_\lambda)$ all lie on a strict warped tree with $m$ twigs and at most $2m - 3$ edges, where $m$ is the number of vertices of* $\mathrm{Conv}(\mathcal{S}_\lambda)$.

Two iterated forests for $\mathcal{Q}_1$ are illustrated below in Figure 32.

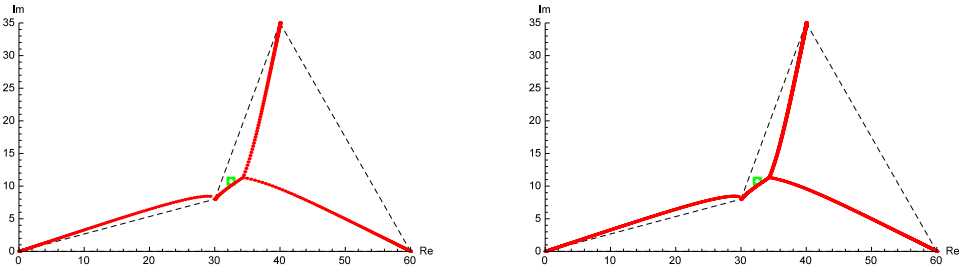


Figure 32: The iterated forests $\mathcal{F}(\mathcal{Q}_1, 100)$ and $\mathcal{F}(\mathcal{Q}_1, 300)$.

The point $30 + 8i$ in the interior of the convex hull of $\mathcal{Q}_1$ is most likely the cause of the apparent discontinuity in $\mathcal{F}(\mathcal{Q}_1, k)$ in Figure 32. Additionally, we should note that because $\mathcal{Q}_1$ is a concave polygon with four vertices, there are actually at least two more polygons $\mathcal{Q}_2$ and $\mathcal{Q}_3$ that give rise to $\mathcal{F}(\mathcal{Q}_1, k)$ (and $\mathcal{V}(\mathcal{Q}_1, k)$). More generally, for any concave polygon $\mathcal{S}$, extra care has to be taken when attempts are made to link properties of the lattice polynomial

$\mathcal{P}(\mathcal{S})$ to the structure of $\mathcal{F}(\mathcal{S}, k)$, because another concave polygon $\mathcal{S}'$ may have more in common with the structure in question.

As an example of such a stronger commonality, let $\mathcal{S}' := \mathcal{Q}_2$ be the quadrilateral whose edges are consecutive pairs of the vertices 0, $40+35i$, 60, $30+8i$, and 0 (which are also the vertices of $\mathcal{Q}_1$). It is noted that the iterated forests in Figure 32 lie entirely inside $\mathcal{Q}_2$. Beyond being the only simple polygon on these vertices with this property, $\mathcal{Q}_2$ also has the largest area among the three possible polygons. In addition, the centroid of $\mathcal{Q}_2$, denoted Centroid $(\mathcal{Q}_2)$, lies closer to Centroid (Conv $(\mathcal{Q}_1)$) than do Centroid $(\mathcal{Q}_1)$ and Centroid $(\mathcal{Q}_3)$.

We illustrate the zeros of $\tilde{p} := \mathcal{P}(\mathcal{Q}_2)$ and its 568th derivative (because $\deg(\hat{p})/568 = 818/568 \approx 720/500$) below in Figure 33.

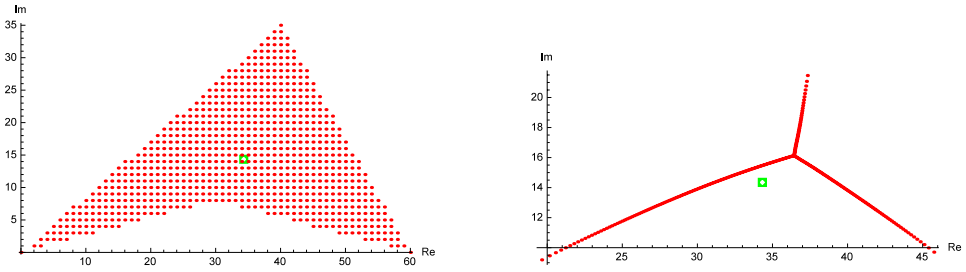


Figure 33: The zeros of $\tilde{p}$ and $\tilde{p}^{(568)}$, where $\deg(\tilde{p}) = 818$.

For completeness, the zeros of $\hat{p} := \mathcal{P}(\mathcal{Q}_3)$ and its 444th derivative are shown below in Figure 34.

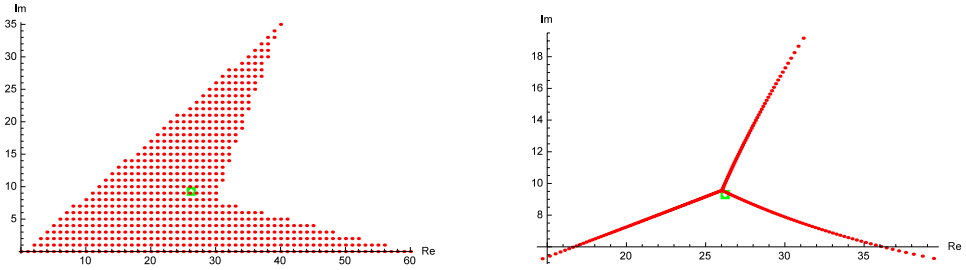


Figure 34: The zeros of $\hat{p}$ and $\hat{p}^{(444)}$, where $\deg(\hat{p}) = 640$.

By comparing figures 31-34, we see that $\mathcal{Z}(\tilde{p})^{(568)}$ looks more similar to $\mathcal{F}(\mathcal{Q}_1, k)$ than do either $\mathcal{Z}(p)^{(500)}$ or $\mathcal{Z}(\hat{p})^{(444)}$, at least based on the directions in which the branches curve. Furthermore, if $\mathcal{S}$ is a polygon with vertices $V$, it may be the case that we will always be able to use $\mathcal{F}(\mathcal{S}, k)$ to find a simple polygon $\mathcal{W}$ among all those with vertices $V$ with some very interesting properties, such as the maximum area, containment of $\mathcal{F}(\mathcal{S}, k)$ in its interior, or a tree structure associated with $\mathcal{P}(\mathcal{W})$ that resembles $\mathcal{F}(\mathcal{S}, k)$

the most.

### 3.3 Pentagons

Inspired by the idea of finding a simple polygon $\mathcal{W}$ on a given set of vertices based on $\mathcal{F}(\mathcal{W}, k)$, we begin with the following definition.

**Definition 3.12.** *Let $V$ be a set of $j \geq 3$ distinct points in the complex plane, and let $S$ be the set of all simple polygons $\mathcal{S}_1, \ldots, \mathcal{S}_m$ whose vertices are $V$. Furthermore, let $\mathcal{W}$ be an element of $S$ such that $\mathcal{W}$ contains $\mathcal{F}(\mathcal{S}_1, k)$ for all $k \in \mathbb{N}$. Whenever $\mathcal{W}$ exists, it is called an intrinsic polygon of $V$, denoted $\mathcal{I}_V$, or an intrisic polygon of $\mathcal{S}_k$, denoted $\mathcal{I}_{S_k}$, $k = 1, \ldots, m$.*

**Remark 3.4.** *Whenever we say 'intrinsic polygon $\mathcal{S}$' without any explicit reference to what $\mathcal{S}$ is an intrinsic polygon of, we are referring to $\mathcal{I}_{\mathcal{S}}$.*

To proceed with our search for intrinsic polygons and their properties, we consider the set $V := \{\alpha_1, \alpha_2, \alpha_3, \alpha_4, \alpha_5\}$ of vertices, where $\alpha_1 = 25$, $\alpha_2 = 80i$, $\alpha_3 = 40 + 35i$, $\alpha_4 = 75 + 50i$, and $\alpha_5 = 80$. By letting $\pentagon_1$ denote the polygon whose edges are consecutive pairs of $\alpha_1$, $\alpha_2$, $\alpha_3$, $\alpha_4$, $\alpha_5$, and $\alpha_1$, which is a concave pentagon whose area is 2912.5, we consider two iterated forests of $\pentagon_1$ below in Figure 35.

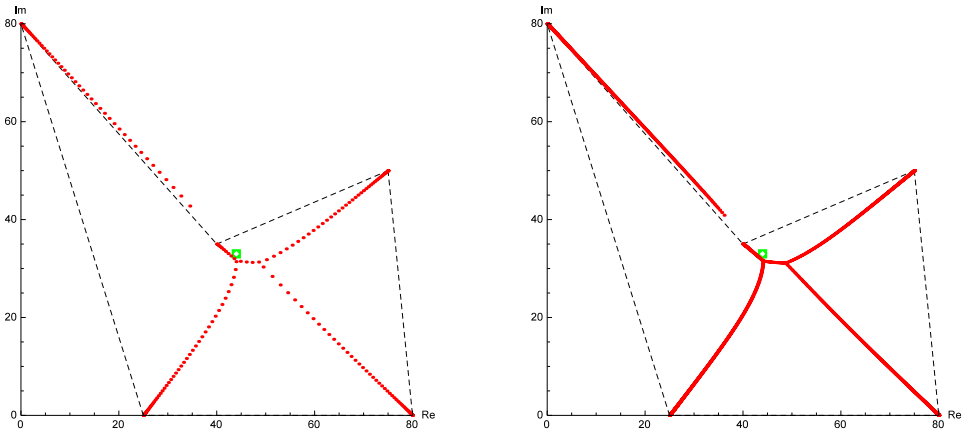


Figure 35: The iterated forests $\mathcal{F}(\pentagon_1, 50)$ and $\mathcal{F}(\pentagon_1, 300)$.

Clearly, $\pentagon_1$ does not capture $\mathcal{F}(\pentagon_1, 50)$ nor $\mathcal{F}(\pentagon_1, 300)$ in its interior, so it is not an intrinsic polygon of $V$. Furthermore, it appears unlikely that the two disjoint parts of $\mathcal{F}(\pentagon_1, k)$ in Figure 35 will merge as $k$ increases. An evident optimization of $\pentagon_1$ that captures both $\mathcal{F}(\pentagon_1, 50)$ and $\mathcal{F}(\pentagon_1, 300)$ in its interior is to define $\pentagon_2$ as the polygon whose edges are consecutive pairs of $\alpha_1$, $\alpha_3$, $\alpha_2$, $\alpha_4$, $\alpha_5$, and $\alpha_1$. To determine whether the trees associated

with $p_2 := \mathcal{P}(\pentagon_2)$ look more similar to $\mathcal{F}(\pentagon_1, k)$ than the trees associated with $p_1 := \mathcal{P}(\pentagon_1)$, consider figures 36 and 37 below.

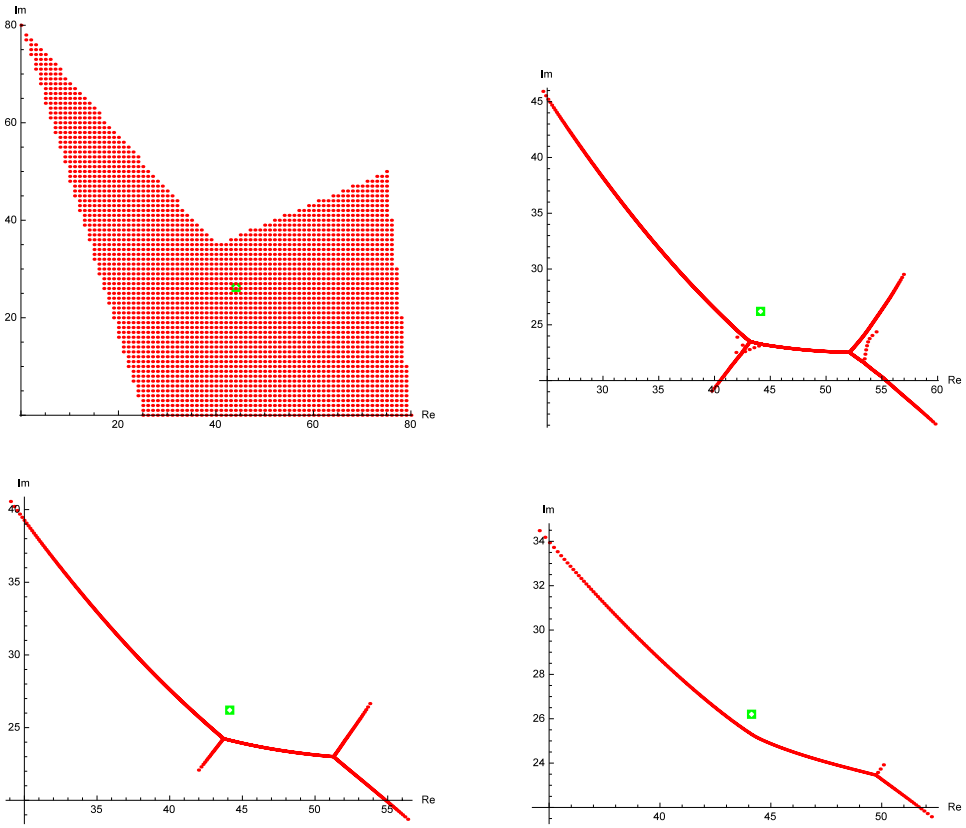


Figure 36: The zeros of $p_1$, $p_1^{(2100)}$, $p_1^{(2400)}$, and $p_1^{(2700)}$, where $\deg(p_1) = 2951$.

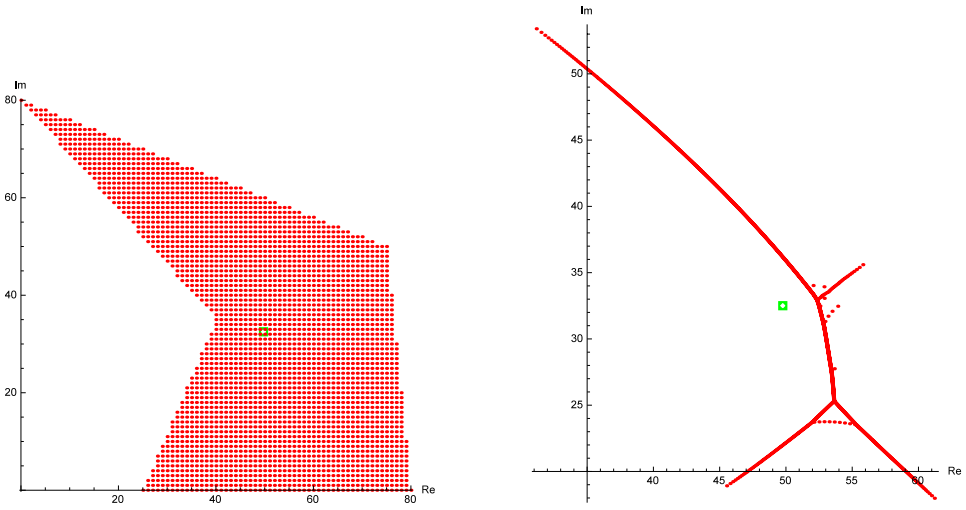


Figure 37: The zeros of $p_2$ and $p_2^{(2139)}$, where $\deg(p_2) = 3006$.

In accordance with Conjecture 3.4 on page 37, figures 36 and 37 show that it does indeed seem to be the convex hull of $\pentagon_\ell$, not $\pentagon_\ell$ itself, that controls the tree structure of $p_\ell^{(k)}$, $\ell = 1, 2$. Furthermore, it is not clear that the zeros of $p_2^{(2139)}$ have a stronger link to $\mathcal{F}(\pentagon_1, k)$ than the zeros of $p_1^{(2100)}$ based on visual appearance.

We proceed by defining $\pentagon_3$ and $\pentagon_4$ on the same five vertices $V$ as those of $\pentagon_1$ (and $\pentagon_2$), which have triangular openings in the convex hull of $V$ in the down and right directions, respectively. Furthermore, let $d_C(S_1, S_2)$ denote the distance between $\text{Centroid}(S_1)$ and $\text{Centroid}(S_2)$. It can be shown that $\text{Area}(\pentagon_1) = 2912.5 < \text{Area}(\pentagon_2) = 2962.5 < \text{Area}(\pentagon_3) = 3037.5 < \text{Area}(\pentagon_4) = 3087.5$, and $d_C(\pentagon_1, \text{Conv}(V)) \approx 7.933 > d_C(\pentagon_2, \text{Conv}(V)) \approx 7.441 > d_C(\pentagon_3, \text{Conv}(V)) \approx 7.365 > d_C(\pentagon_4, \text{Conv}(V)) \approx 6.870$. In other words, the intrinsic polygon $\pentagon_2$ of $V$ does not have the largest area, nor the centroid closest to the centroid of $\text{Conv}(V)$. Thus, unlike the case for the intrinsic polygon $\mathcal{Q}_2$ in the previous section, we cannot expect the largest area, nor the closest centroid to that of the convex hull in the general case. It should be noted, however, that the polygon $\pentagon_4$ with these properties, traps the smallest number of edges (and the fewest zeros) of $\mathcal{F}(\pentagon_1, k)$, so we refrain from ruling out a more elaborate link of these properties. In addition, the two intrinsic polygons $\mathcal{Q}_2$ and $\pentagon_2$ discussed so far have been unique for their respective vertices.

To further test the uniqueness of intrinsic polygons, we let $\widetilde{\pentagon}_1, \ldots, \widetilde{\pentagon}_8$ be the eight simple pentagons that can be defined on the vertices $\beta_1 = 25$, $\beta_2 = 90i$, $\beta_3 = 50 + 60i$, $\beta_4 = 90 + 70i$, and $\beta_5 = 35 + 35i$. We illustrate the vertex set of $\widetilde{\pentagon}_k$, and the iterated forests $\mathcal{F}(\widetilde{\pentagon}_k, 300)$, $k = 1, \ldots, 8$ below in Figure

38.

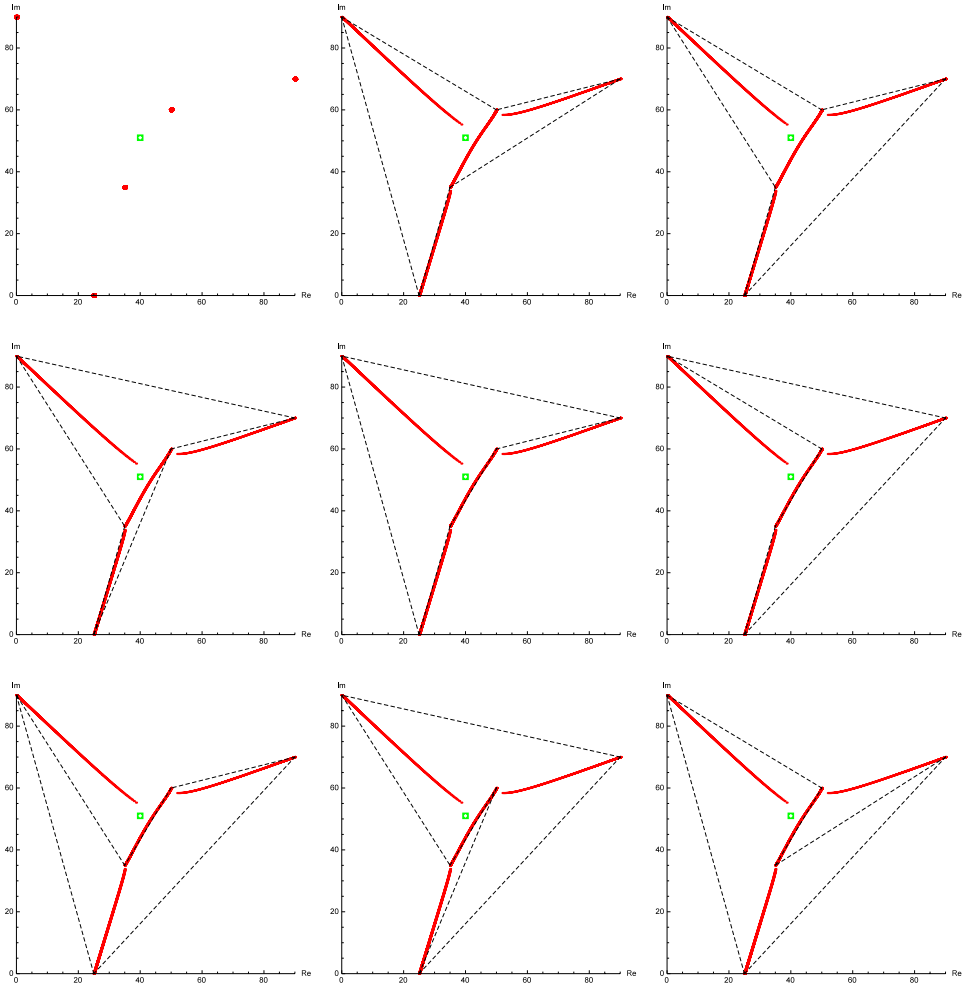

Figure 38: The vertex set of $\widetilde{\hexagon}_k$, and the iterated forests $\mathcal{F}(\widetilde{\hexagon}_k, 300)$, $k = 1, \ldots, 8$. Note that if the curve between $\beta_3$ and $\beta_5$ exists as a single warped curve in the intrinsic forest $\mathcal{F}(\widetilde{\hexagon}_k)$, then it is unlikely to be strict. Furthermore, the centroid of $\widetilde{\hexagon}_2$ is closest to that of its convex hull.

As seen in Figure 38, we yet again seem to get a single intrinsic polygon of $V$, namely $\widetilde{\hexagon}_2$, where $V$ denotes the vertices of $\widetilde{\hexagon}_1, \ldots, \widetilde{\hexagon}_8$. Consequently, we formulate the following conjecture.

**Conjecture 3.5.** *Let $\mathcal{S}$ be a polygon with vertices $V$ and center of mass $m$ of its vertices. If no three elements of $V \cup \{m\}$ are collinear, then there is a unique intrinsic polygon $\mathcal{I}_S$ of $\mathcal{S}$.*

**Remark 3.5.** *The collinearity requirement arises because if $\mathcal{S}_1, \ldots, \mathcal{S}_4$ denote the four concave polygons with vertex set $V = \{0, \pm 1 \pm i\}$, then the*

*iterated forests of either of these polygons lie on the diagonals of* $\mathrm{Conv}\,(V)$ *for reasons of symmetry. Consequently,* $\mathcal{S}_1, \ldots, \mathcal{S}_4$ *are all intrinsic polygons of* $V$*. Similarly, symmetries over lines containing* $m$ *and two zeros can give rise to trivial non-uniqueness.*

**Remark 3.6.** *Conjecture 3.5 can be seen as a version of the Gauss-Lucas theorem that works for derivatives of order* $k$ *for* $\mathcal{V}(\mathcal{S}, k)$*. It is likely that the zeros stay inside the intrinsic polygon for any order of the derivative.*

We content ourselves with displaying the zeros of $\breve{p} := \mathcal{P}(\widetilde{\pentagon}_1)$ and its 1700th derivative below in Figure 39, where we see that the number of branches (or possibly twigs on the warped tree) is equal to the number of vertices of $\mathrm{Conv}\,(\widetilde{\pentagon}_1)$; see Conjecture 3.4.

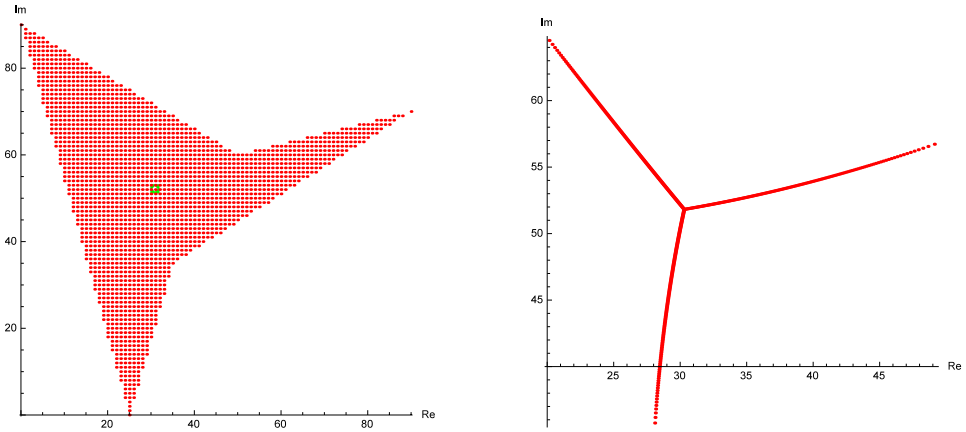


Figure 39: The zeros of $\breve{p}$ and $\breve{p}^{(1700)}$, where $\deg\,(\breve{p}) = 2181$.

Returning to convex polygons, let $\pentagon$ denote the pentagon with corners at the points 10, $36i$, $29 + 58i$, $58 + 36i$, and 48, which is not regular, but has symmetry over the line $\mathrm{Re}\; z = 29$. Furthermore, we form $\widehat{\pentagon}$ from $\pentagon$ by moving the vertex 48 to 50, creating a minute asymmetry. Subsequently, we define $p := \mathcal{P}(\pentagon)$ and $q := \mathcal{P}(\widehat{\pentagon})$, which have degrees 2389 and 2427, respectively. The situation is illustrated below in figures 40 and 41, where we see that the relatively small asymmetry has shifted one of the twigs down the 'trunk', and divided the latter into two connected segments.

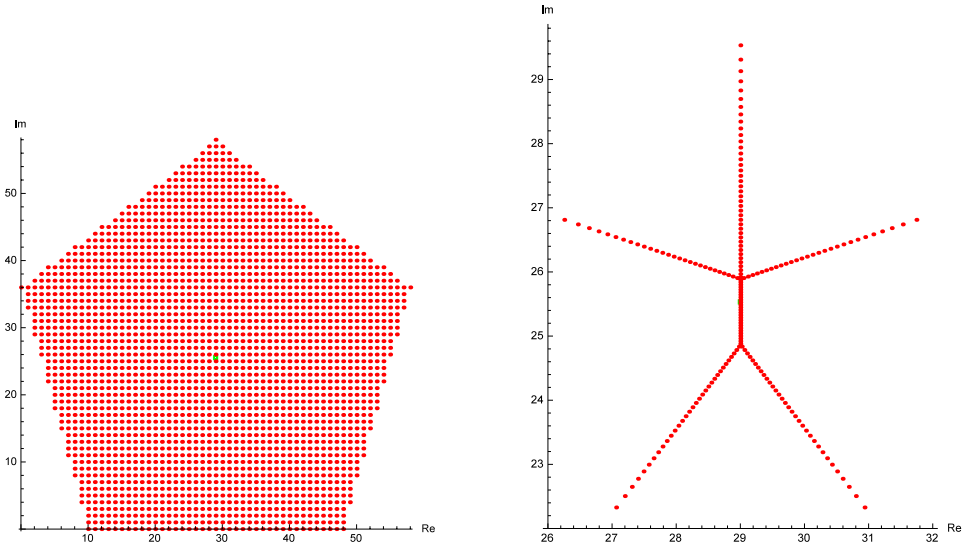


Figure 40: The zeros of $p$ and $p^{(2200)}$.

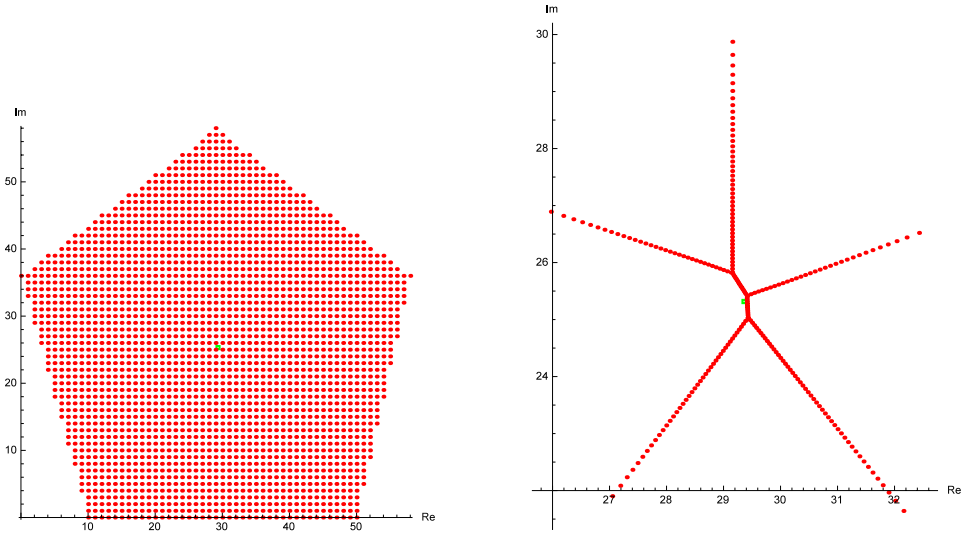


Figure 41: The zeros of $q$ and $q^{(2200)}$.

The seven edges in Figure 41 are in accordance with the maximum of $2n-3$ edges we have previously seen for tree structures associated with concave $n$-gons (see Conjecture 3.4, page 37). Two iterated forests for the pentagons $\pentagon$ and $\widehat{\pentagon}$ are shown below in Figure 42.

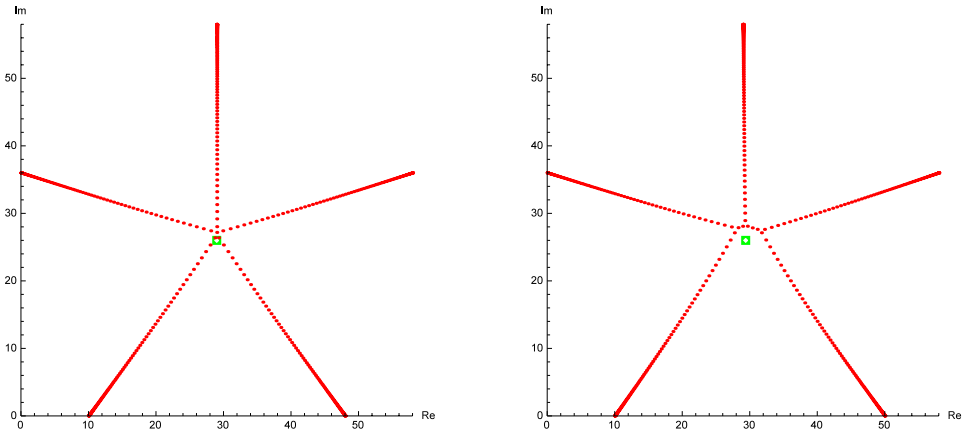


Figure 42: The iterated forests $\mathcal{F}(\pentagon, 100)$ and $\mathcal{F}(\widehat{\pentagon}, 100)$.

Curiously, $\mathcal{F}(\widehat{\pentagon}, 100)$ in Figure 42 roughly has the appearance of a $72\,^\circ$ counterclockwise rotation of $\mathcal{Z}(q^{(2200)})$ in Figure 41. This gives some indication that the distribution of zeros inside a polygon has a relatively nice map to the associated tree structure. Additionally, we note that the tree structures in the figures bear resemblance to the support of the mother body of a convex pentagon.[5] The support of a pentagon $\dot{\pentagon}$ is compared to an iterated forest generated from a polynomial with its zeros approximately in the vertices of $\dot{\pentagon}$ below.

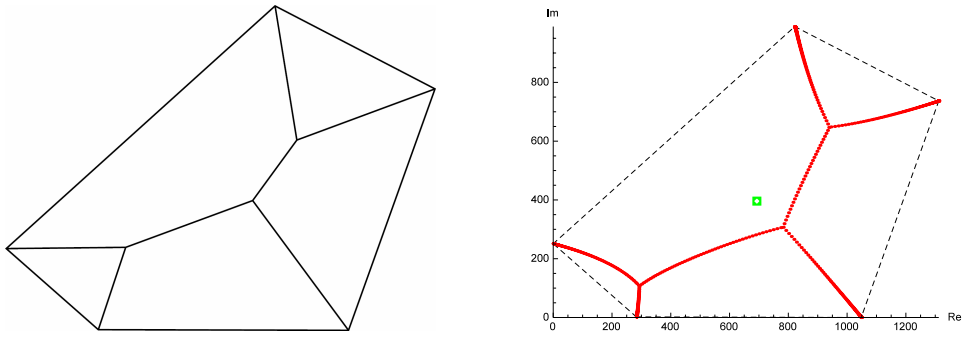


Figure 43: The support of the mother body $\dot{\pentagon}$, and the iterated forest $\mathcal{F}(\dot{\pentagon}, 100)$.

As seen in Figure 43, the iterated forest $\mathcal{F}(\tilde{\pentagon}, 100)$ shares similarities with the support for $\tilde{\pentagon}$, while the structures are obviously not identical.

### 3.4 Simple polygons with six or more sides

Determined to delve deeper into the properties of intrinsic polygons, and further test the validity of Conjecture 3.5, we start this section by generating eight separate sets $V_1, \ldots, V_8$ of random Gaussian integers, such that no three elements of $V_\ell \cup \{m_\ell\}$ are collinear, where $m_\ell$ are the respective centers of mass of $V_\ell$, $\ell = 1, \ldots, 8$. Eight iterated forests $\mathcal{F}(\triangle_\ell, k)$ are shown below in figures 44-47 for various values of $k$, where $\triangle_\ell$ is the unique, simple polygon with vertices $V_\ell$ that contains $\mathcal{F}(\triangle_\ell, k)$, $\ell = 1, \ldots, 8$.

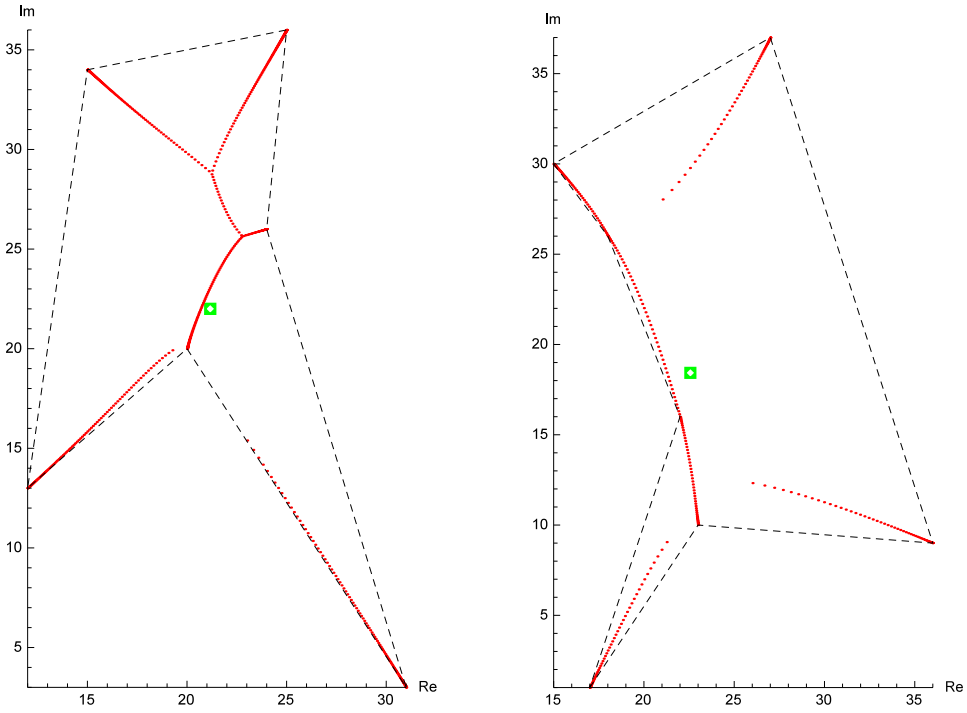


Figure 44: The iterated forests $\mathcal{F}(\triangle_1, 100)$ and $\mathcal{F}(\triangle_2, 50)$, where $\triangle_1$ and $\triangle_2$ are hexagons and heptagons, respectively.

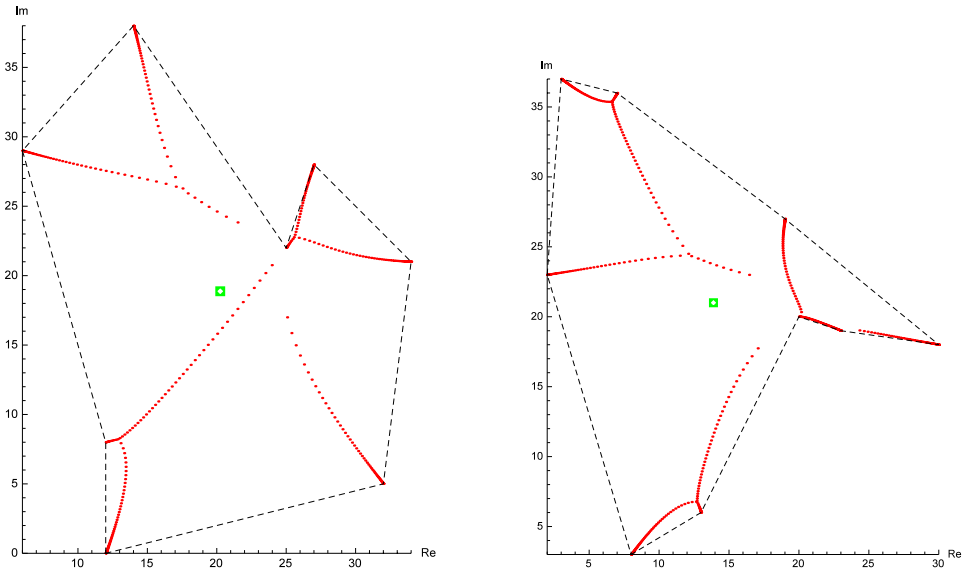


Figure 45: The iterated forests $\mathcal{F}(\triangle_3, 50)$ and $\mathcal{F}(\triangle_4, 50)$, where $\triangle_3$ and $\triangle_4$ are octagons and nonagons, respectively.

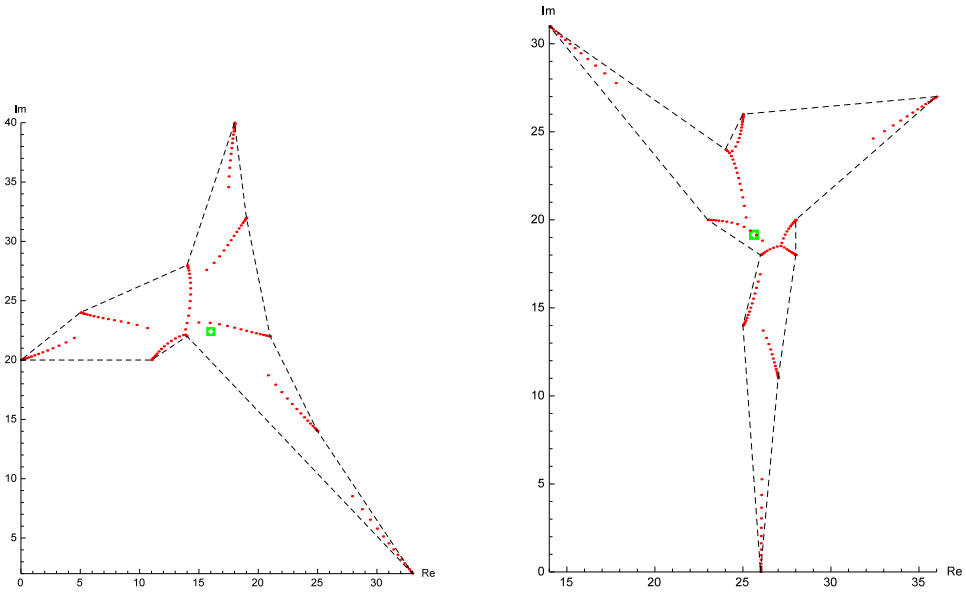


Figure 46: The iterated forests $\mathcal{F}(\triangle_5, 15)$ and $\mathcal{F}(\triangle_6, 15)$, where $\triangle_5$ and $\triangle_6$ are decagons and hendecagons, respectively.

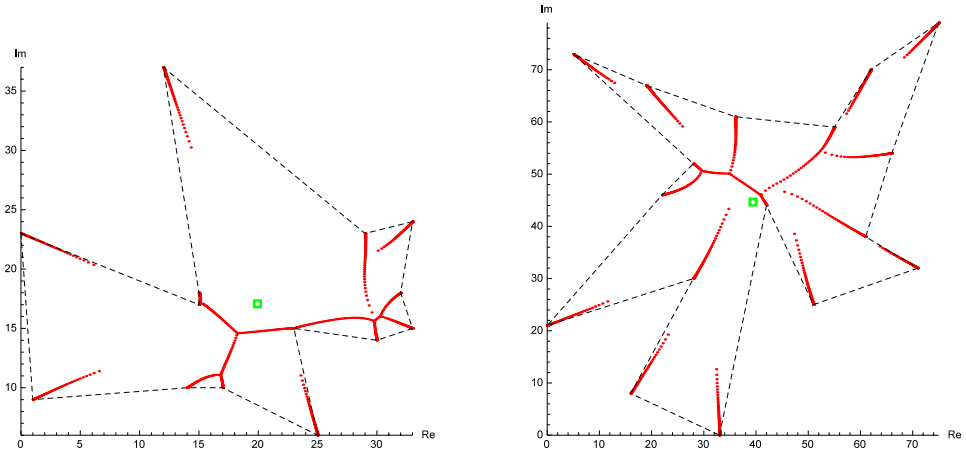


Figure 47: The iterated forests $\mathcal{F}(\triangle_7, 50)$ and $\mathcal{F}(\triangle_8, 50)$, where $\triangle_7$ and $\triangle_8$ are tetradecagons and heptadecagons, respectively.

We finish this section with a few illustrations of the zeros of four different lattice polynomials $p$ and their derivatives, as shown below in figures 48-51.

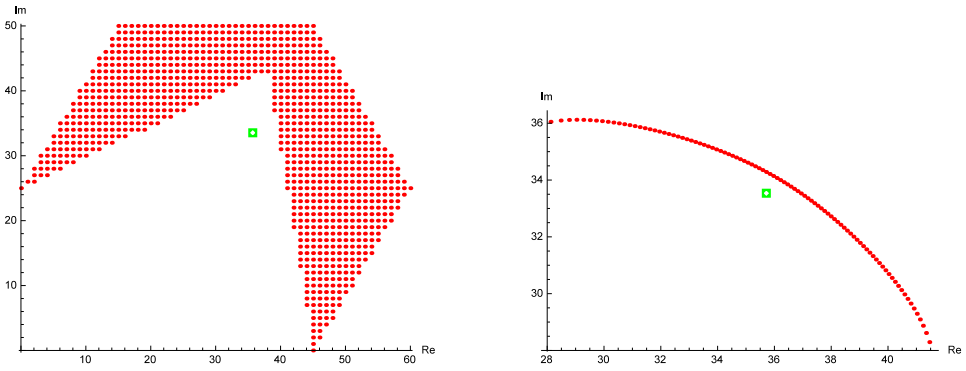


Figure 48: The zeros of $p$ and $p^{(925)}$, where $\deg(p) = 1020$.

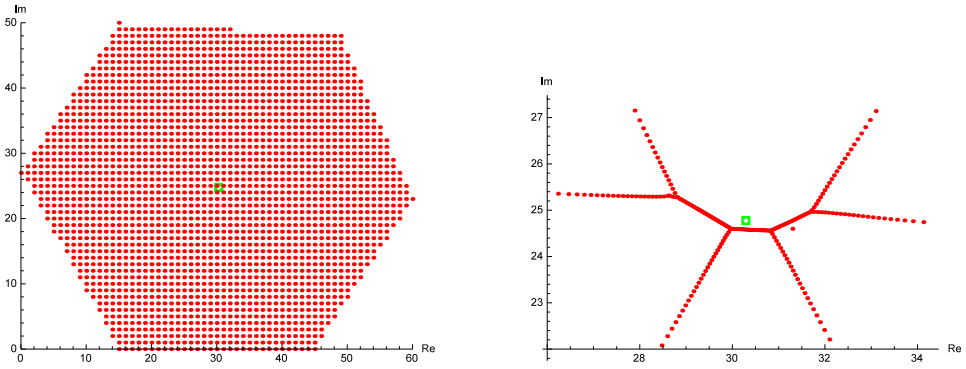


Figure 49: The zeros of $p$ and $p^{(2066)}$, where $\deg(p) = 2279$.

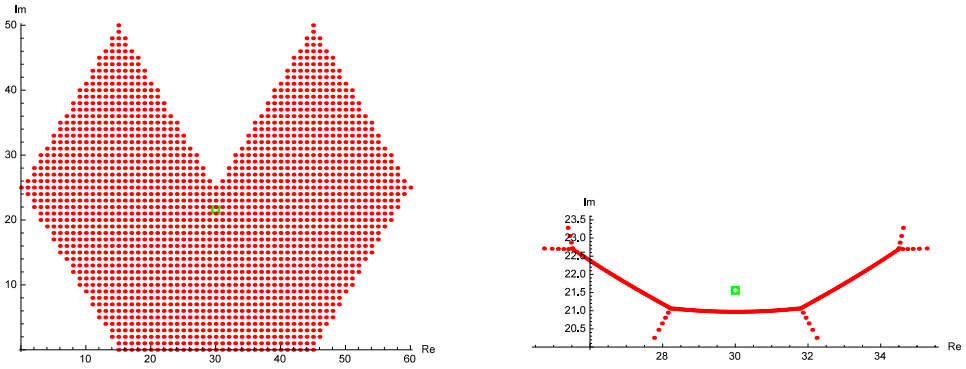


Figure 50: The zeros of $p$ and $p^{(1728)}$, where $\deg(p) = 1906$.

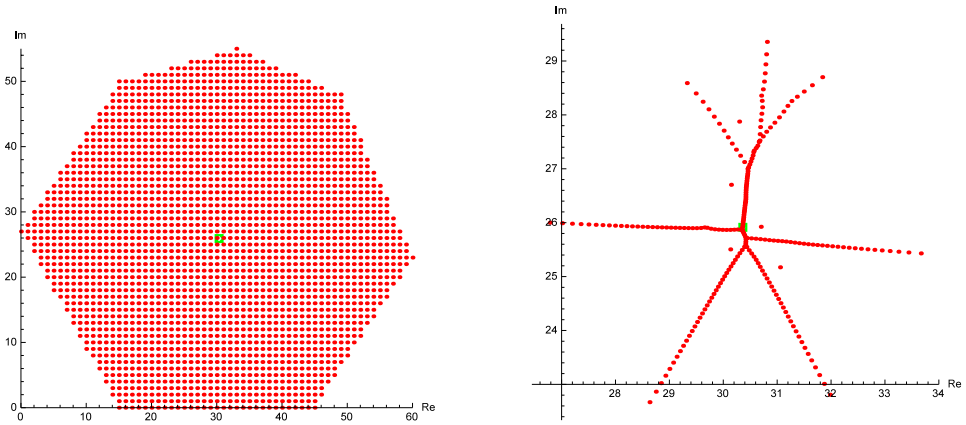


Figure 51: The zeros of $p$ and $p^{(2159)}$, where $\deg(p) = 2382$.

Again, the claim in Conjecture 3.4 about the emergence of at most $2m - 3$ edges in the tree of a simple $m$-gon's lattice polynomial appears to be valid.

### 3.5 Tree stability and general experiments

In this last part of section 3, we will experiment with a few polynomials related to the ones previously considered, such as lattice polynomials defined on irregular shapes, and polynomials with zeros on specific curves. To probe the nature of the tree structures in earlier sections further, we begin by considering the polynomial $p := ((z-6)(z+6)(z-15i))^{140}$. The zeros of $p$ define an isosceles triangle similar to the one in Figure 28 on page 35. Unlike the last time, however, we will differentiate $p$ beyond the order of when its zeros form an iterated tree with three branches, and consider what happens to the point $w = w(d)$ where its three branches meet, as seen below in Figure 52.

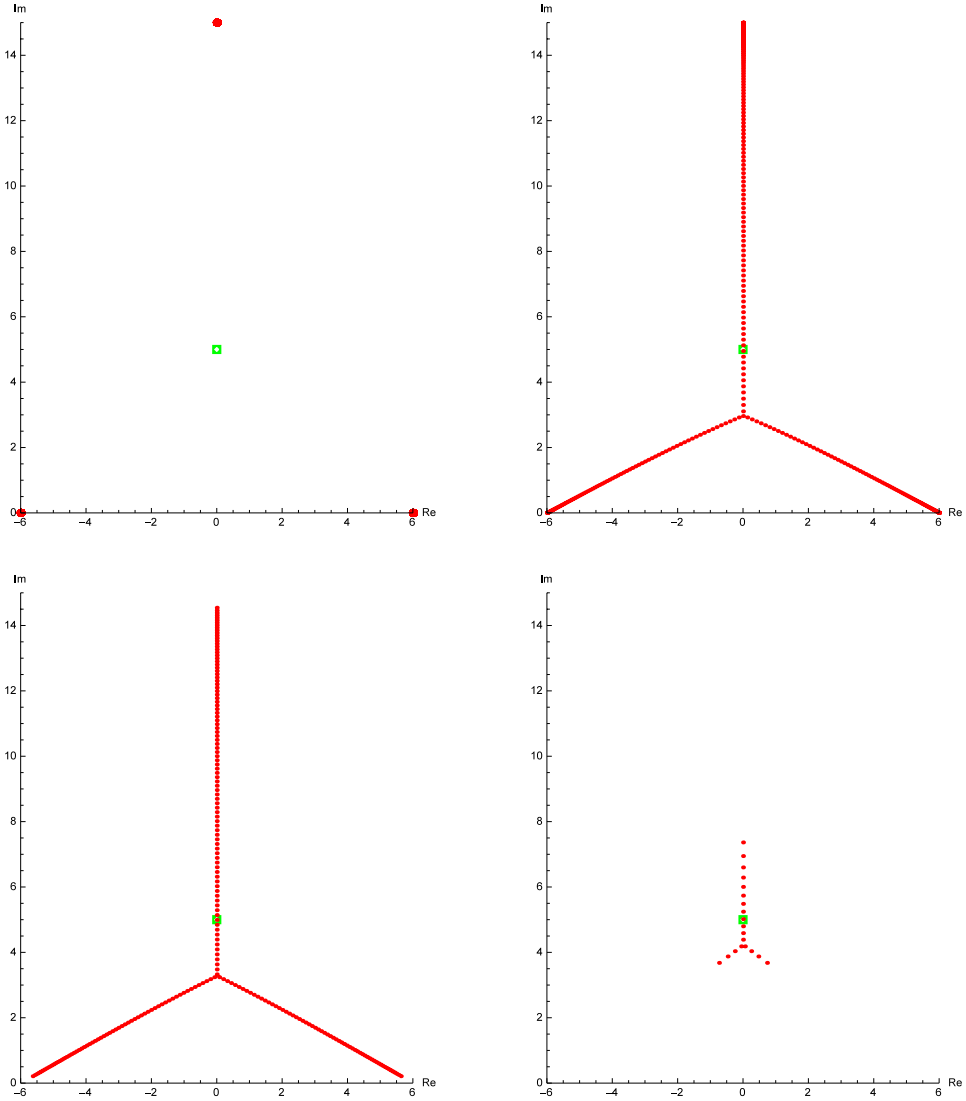


Figure 52: The zeros of $p$, $p^{(139)}$, $p^{(200)}$ and $p^{(400)}$, where $\deg(p) = 420$.

Because it is difficult to determine the position of $w$ exactly for any fixed order $d$ of the derivative, we consider the point $w' = w'(d)$ instead, which is the zero of $p^{(d)}$ on the imaginary axis closest to the origin. Furthermore, we let $a = a(d)$ and $b = b(d)$ denote the number of zeros of $p^{(d)}$ that lie on and not on the imaginary axis, respectively (so that $a + b = \deg(p^{(d)})$). The distance to $w'$ from the origin, and the values of $a$ and $b$, are plotted for $340 \leq d \leq 419$ below in Figure 53.

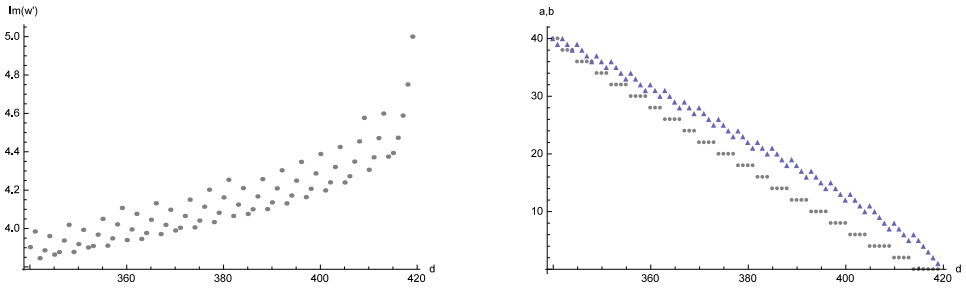


Figure 53: The values of $\mathrm{Im}(w')$ (left), and the values of $a$ (triangles) and $b$ (disks) (right), for various orders $d$ of the derivative.

Figure 53 shows that the average tendency of $w'$ to move closer to the center of mass $5i$ of the zeros is punctuated by smaller cycles of movement. Specifically, during each cycle, $w'$ moves away from the origin at an accelerating pace, while the number of zeros on the branches mirrored over the imaginary axis remains constant. Only zeros on the imaginary axis are removed during the cycle. When the cycle ends, a zero from each of the two symmetrical branches is removed, while a zero is added to the imaginary axis. This can be seen as the two zeros on the symmetrical branches closest to the imaginary axis merging and becoming a new zero $w'$, resetting its position and velocity.

Before we proceed to another polynomial, let $\mu_x = \mu_x(d)$ and $\mu_y = \mu_y(d)$ denote the width and height of the convex hull of the zeros of $p^{(d)}$, respectively. The values of $\mu_x$ and $\mu_y$ are plotted for $340 \leq d \leq 419$ below in Figure 54.

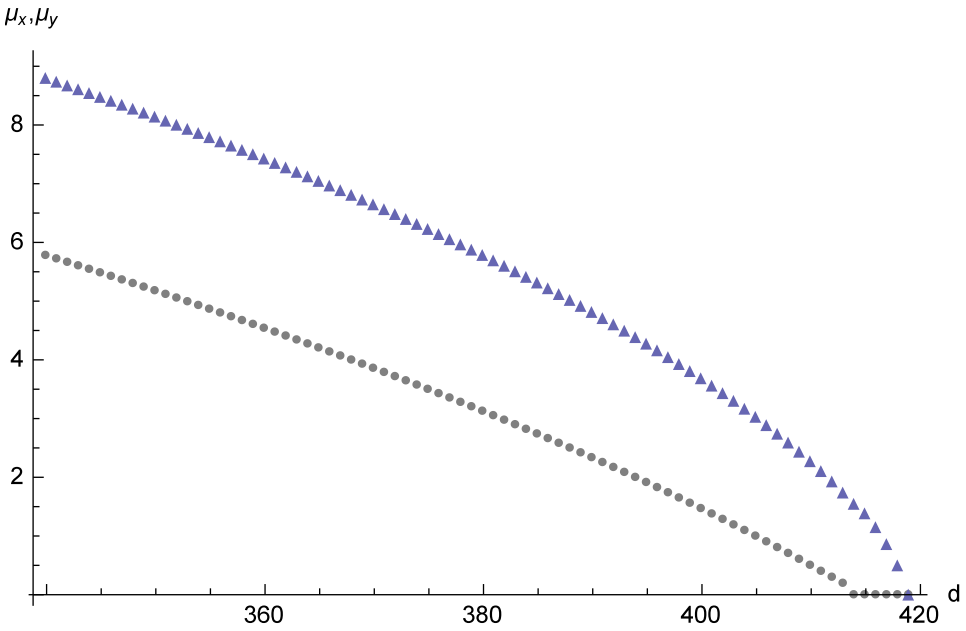


Figure 54: The width $\mu_x$ (disks) and height $\mu_y$ (triangles) of Conv $(\mathcal{Z}(p^{(d)}))$.

It can be discerned from Figure 54 that the collapse of the symmetrical branches of $\mathcal{Z}(p^{(d)})$ at $d = 414$ changes the rate at which $\mu_y$ decreases. Thus, the situation is analogous to previous collapses of zeros onto lines (see the discussions after figures 5 and 16, respectively).

Continuing with the theme of triangles, let $\hat{p}$ be a polynomial with 14 zeros, each of multiplicity 30, such that 13 of them are distributed in the lattice points $-6, -5, \ldots, 6$, and allow its 14th zero $z(\kappa)$ to move along the imaginary axis, $\kappa \in \mathbb{R}$. Explicitly, $\hat{p}$ is given by

$$\hat{p} := \left( (z - \kappa i) \prod_{\ell=-6}^{6} (z - \ell) \right)^{30}. \tag{42}$$

Similarly to the polynomial $p$ in Figure 52, we will consider what happens to the zeros of $\hat{p}$ when $\hat{p}$ is differentiated more than 29 times; see Figure 55 below.

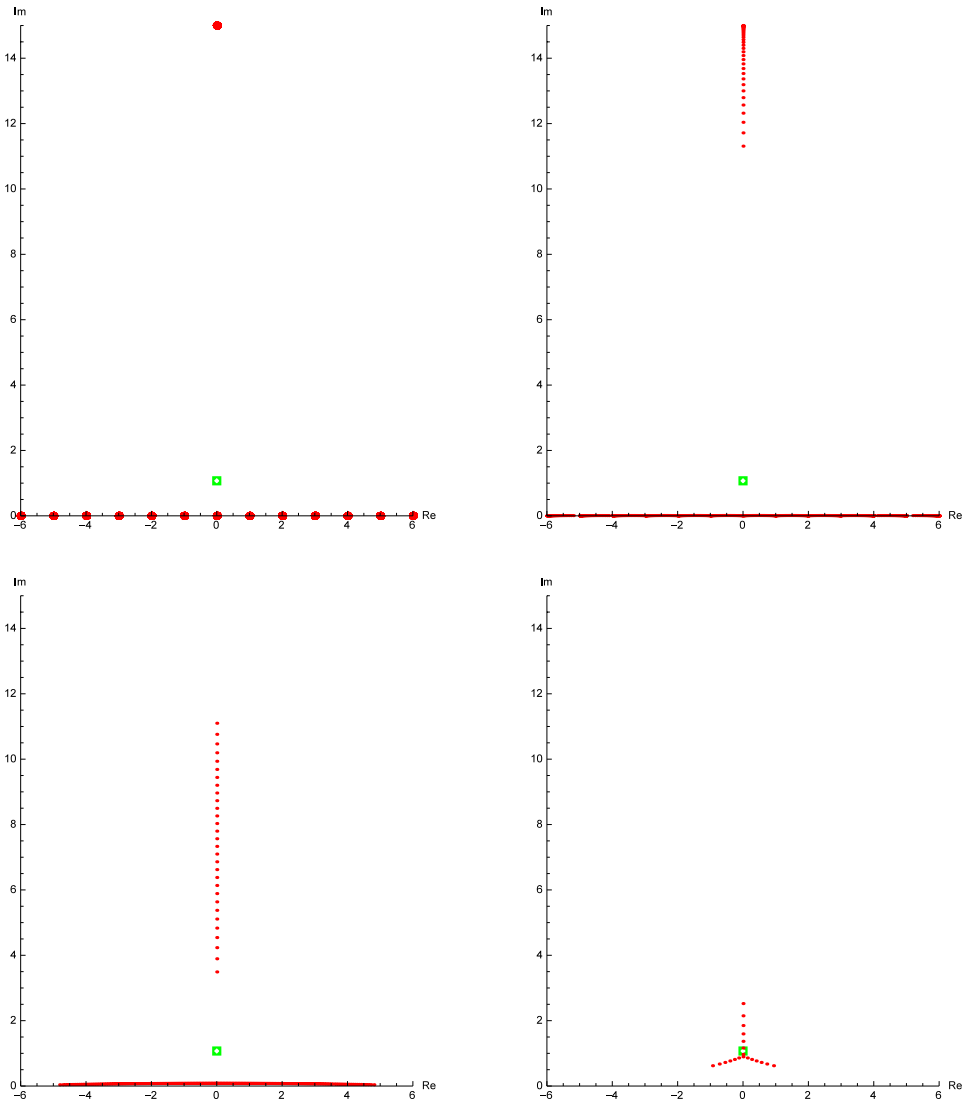


Figure 55: The zeros of $\hat{p}$, $\hat{p}^{(29)}$, $\hat{p}^{(200)}$ and $\hat{p}^{(400)}$, where $\deg(\hat{p}) = 420$. Here, $\kappa = 15$.

Evidently, Figure 55 shows that the branch of zeros of $\hat{p}^{(29)}$ that emerged from $z(\kappa)$ has travelled down toward the zeros closer to the real axis in $\hat{p}^{(200)}$. Furthermore, these zeros have travelled as a cohesive unit, with their spacing more equalized than previously. Eventually, all remaining zeros have amalgamated around a common point $w$, from which three separate branches of zeros emerge, as seen for $\hat{p}^{(400)}$.

An inquiry into the stability of $w$ with respect to different orders $d$ of the derivative shows similar cycles to the ones exhibited in Figure 53. We proceed differently by letting $w' = w'(\kappa)$ denote the zero of $\hat{p}^{(400)}$ on the imaginary axis with the smallest imaginary part. Furthermore, analogously to the previous situation for $p$, we let $a = a(\kappa)$ and $b = b(\kappa)$ denote the number of zeros of $\hat{p}^{(400)}$ that lie on and not on the imaginary axis, respectively, so $a + b = \deg(\hat{p}^{(400)}) = 20$. By increasing the value of $\kappa$ from 0 to 70 in integer increments, we get the following plot of the imaginary part of $w'$ below in Figure 56, shown next to a plot of $a$.

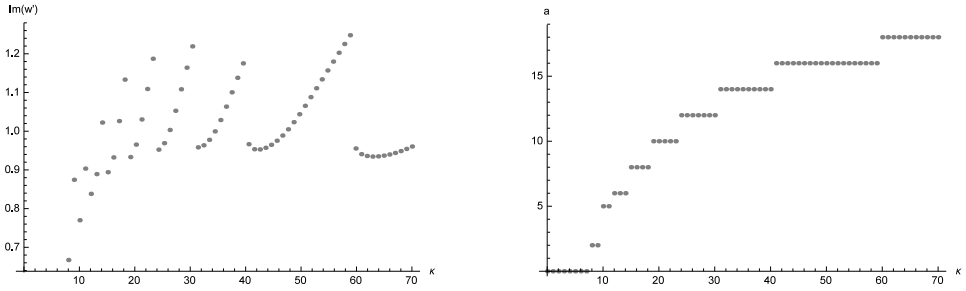


Figure 56: The imaginary part of $w'$ (left), and the number of zeros in the tree of $\hat{p}^{(400)}$ that lie on the imaginary axis (right), for different values of $\kappa$.

Figure 56 shows that $w'$ tends to diverge away from the origin toward larger numbers on the imaginary axis as $\kappa$ increases. As might have been expected, a cyclic pattern of this divergence appears, in which $w'$ jumps back toward the origin whenever zeros of $\hat{p}^{(400)}$ disappear from the two (roughly) horizontal branches and are added to the imaginary axis. It is less apparent why the 'momentum' of this jump toward the real axis is maintained by $w'$ for a few steps of $\kappa$.

To investigate how the density of zeros in the lower branch of $\hat{p}$ affects the 'train' of zeros on the imaginary axis in Figure 55, we let $\alpha$ be a real number, and define

$$\tilde{p} := \left( (z - \kappa i) \prod_{\ell=-6}^{6} (z - \alpha\ell) \right)^{30} . \tag{43}$$

The zeros of $\tilde{p}^{(200)}$ are shown below in Figure 57 for various values of $\alpha$.

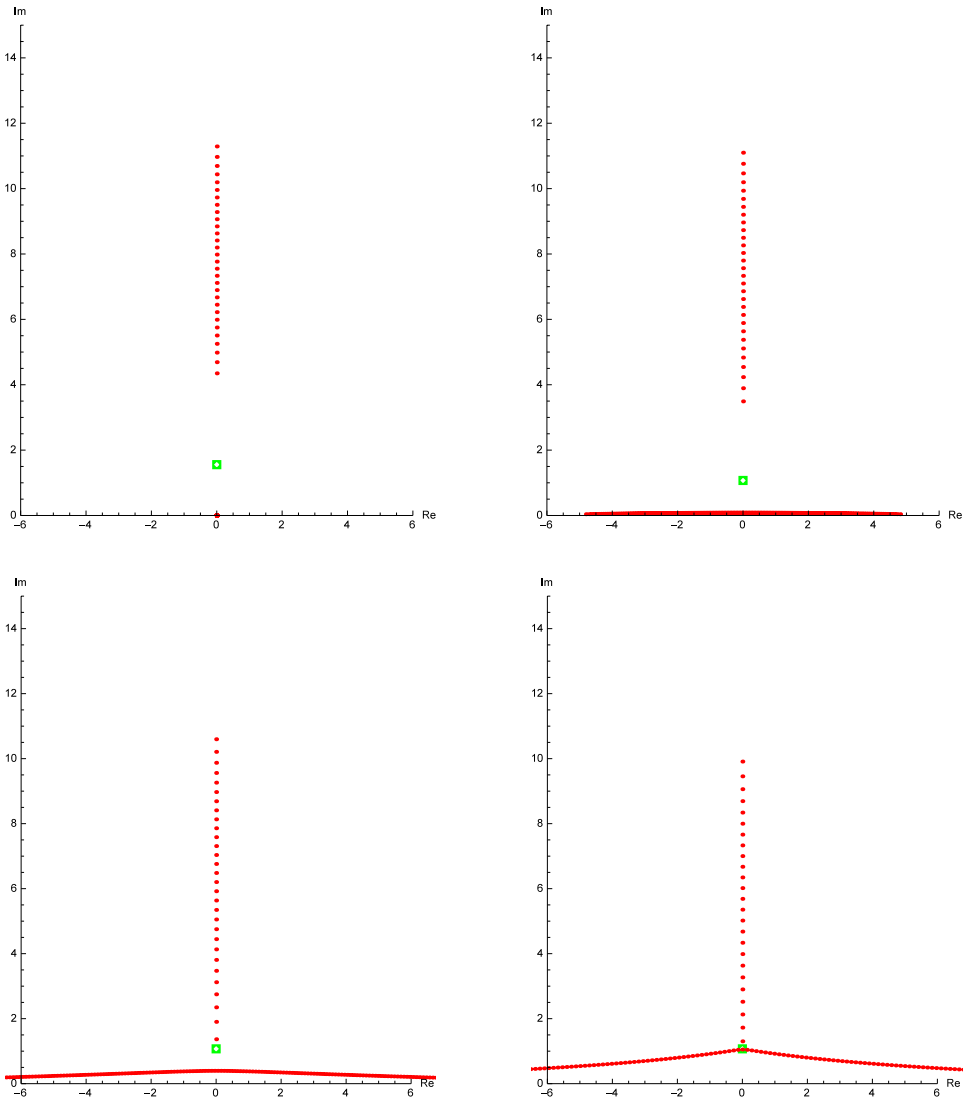


Figure 57: The zeros of $\tilde{p}^{(200)}$, when $\kappa = 15$ and $\alpha = 0, 1, 2, 3$. Note that some zeros are outside the plot range when $\alpha = 2, 3$.

Clearly, increasing $\alpha$ extends the length of the 'train' and shifts it toward the real axis. Analogously, it might be interesting to investigate how much various two-dimensional shapes composed of simple zeros are shifted and deformed by zeros of higher multiplicities at various distances.

We proceed by letting $D_1$ be the circular disk with radius 30 centered around the origin, and let $D_2$ be the circular disk with radius 15 centered around the point $8i$. We let $p := \mathcal{P}(D_1 \setminus D_2)$, and illustrate the zeros of $p$ and some of its derivatives below in Figure 58.

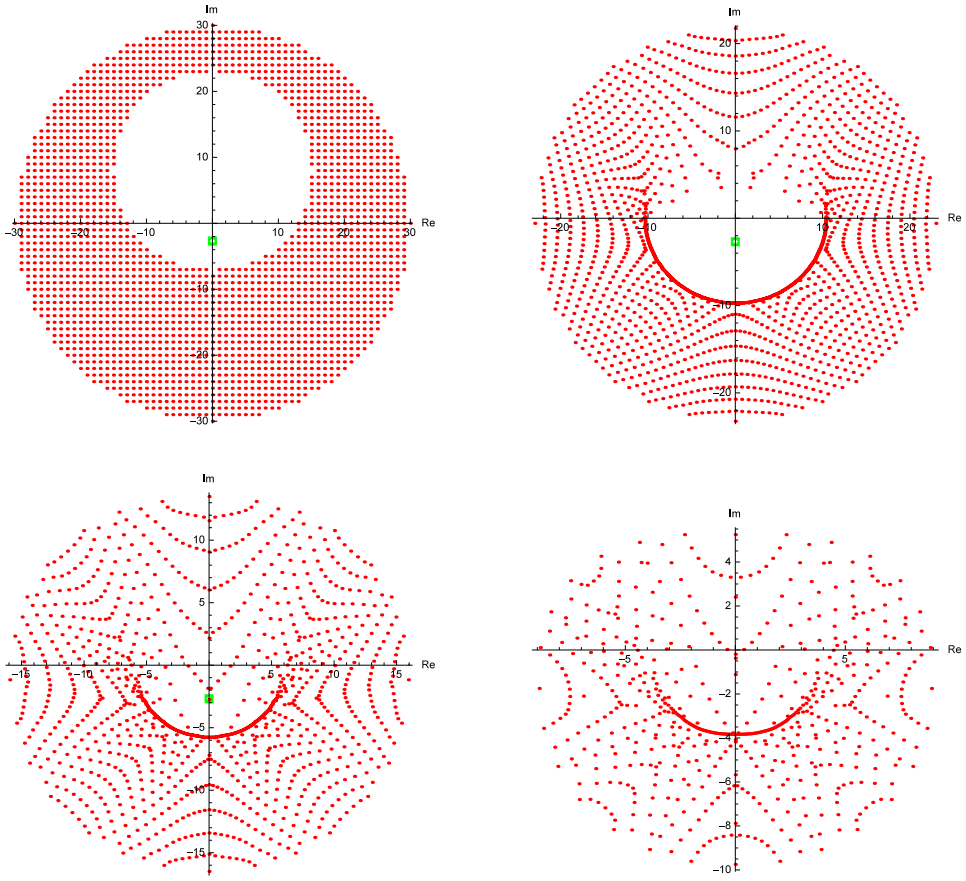


Figure 58: The zeros of $p$, $p^{(400)}$, $p^{(800)}$, and $p^{(1200)}$, where $\deg(p) = 1407$.

We continue by considering the circular sector $C$ given by the points $z = re^{i\theta}$, where $0 \leq r \leq 50$ and $\pi/3 \leq \theta \leq 2\pi/3$. The zeros of $p := \mathcal{P}(C)$ and some of its derivatives are shown below in Figure 59.

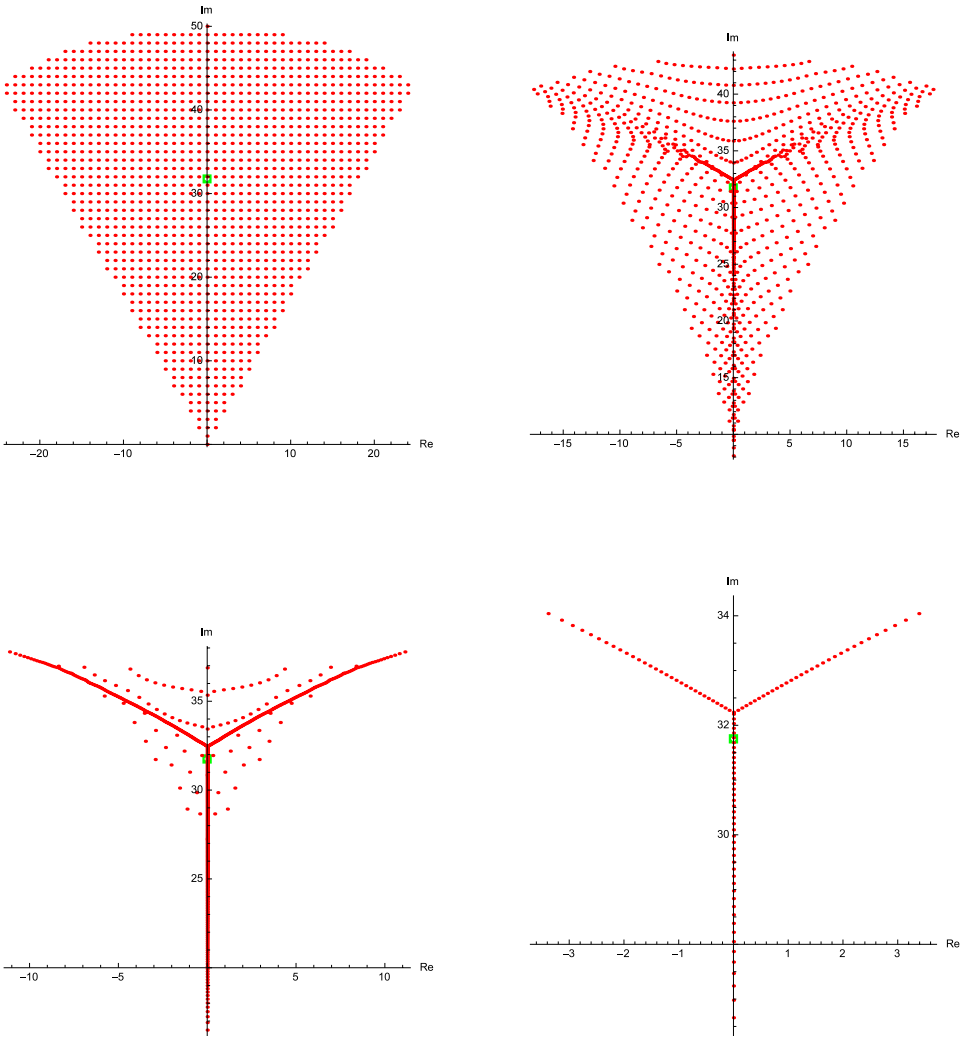


Figure 59: The zeros of $p$, $p^{(400)}$, $p^{(800)}$, and $p^{(1200)}$, where $\deg(p) = 1307$.

Next, we consider an elliptical disk $D$ with minor and major axes 15 and 30, respectively, and as usual, let $p := \mathcal{P}(D)$; see Figure 60.

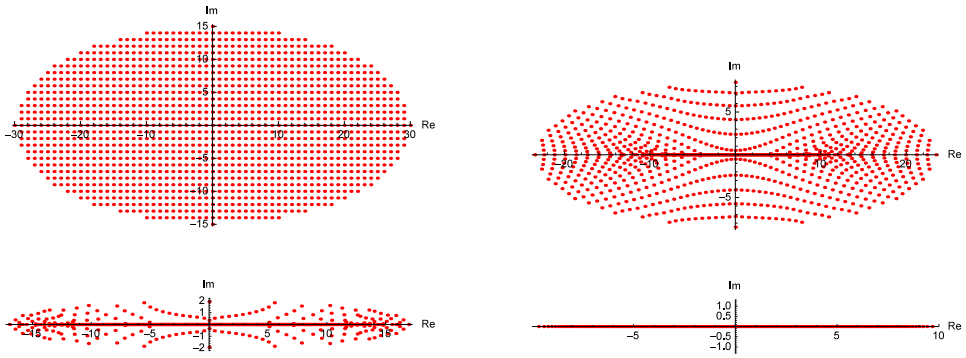


Figure 60: The zeros of $p$, $p^{(400)}$, $p^{(800)}$, and $p^{(1200)}$, where $\deg(p) = 1407$.

The fields of forces described in Theorem A.1 are exhibited in Figure 61, where $p$ is a polynomial with 121 zeros, each of multiplicity 5, in the ellipse $z = 8\cos(x) + 5i\sin(x)$, $0 \leq x < 2\pi$. Slightly uneven distribution of zeros, rather than numerical instability, causes the asymmetry displayed.

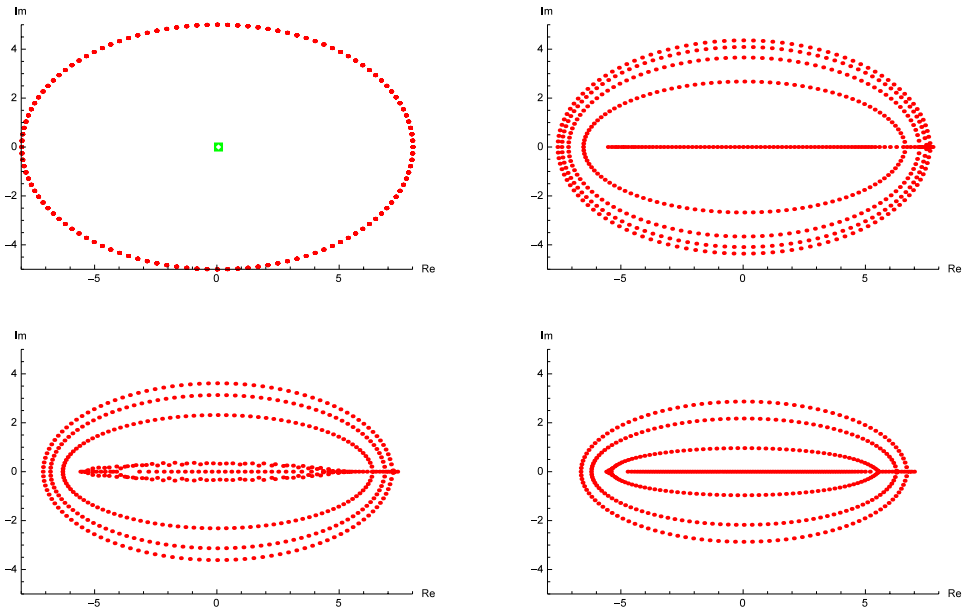


Figure 61: The zeros of $p$, $p^{(50)}$, $p^{(100)}$, and $p^{(150)}$, where $\deg(p) = 605$.

We continue by creating a polynomial $p$ whose simple zeros lie approximately on a period of a sine curve. Specifically, we define $p$ as

$$p := \prod_{k=-31}^{31} (z - (k + i \cdot \operatorname{nint}(60\sin(k/10)))), \tag{44}$$

where $\operatorname{nint}(x)$ is the nearest integer function that returns the integer closest

to $x \in \mathbb{R}$. The situation for the zeros of $p$ and some of its derivatives is shown below in Figure 62.

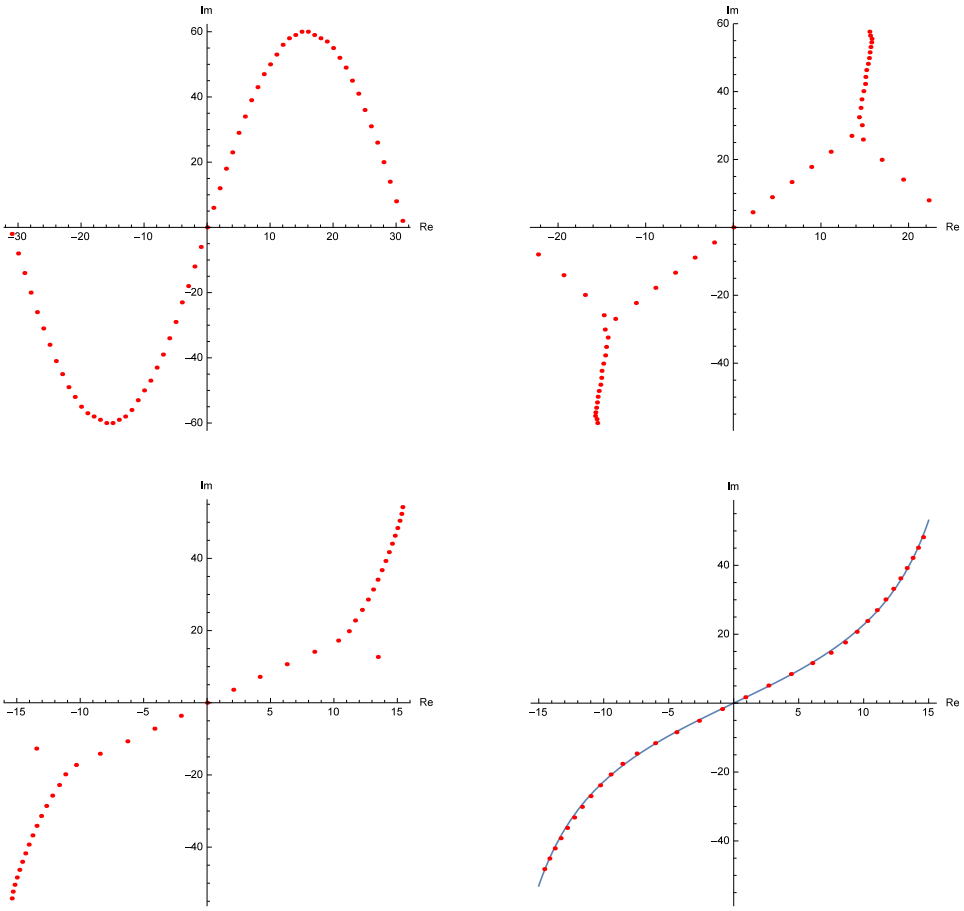


Figure 62: The zeros of $p$, $p^{(10)}$, $p^{(20)}$, and $p^{(31)}$, where $\deg(p) = 63$. The curve shown is given by $z = x + 23.5\tan(x/13)i$, $x \in \mathbb{R}$.

Strangely, Figure 62 shows that the derivative of order $\lfloor \deg(p)/2 \rfloor$ gives rise to what appears to be a tangent curve, which even seems to have approximately half the period of the initial sine curve.

Finally, we consider polynomials $p$ with distinct, simple zeros again. Previously, we raised $p$ to the $n$:th power (for some natural number $n$), followed by $n$ differentiations, which gave rise to iterated forests for the resulting polynomials $(p^n)^{(n)}$. By replacing the $n$ differentiations with $n$ times repeated antidifferentiations (and setting the integration constant to 0 each time), different zero distributions emerge. Specifically, the zeros for these polynomials, which we may denote $(p^n)^{(-n)}$, appear to form forests whose edges are smooth curves when $n \to \infty$, similarly to what we saw for iterated

forests. We illustrate a few zero distributions for $(p^n)^{(-n)}$ for various $p$ and $n$ below in figure 63, where the original polynomial $p$ in each case has zeros indicated by the larger disks.

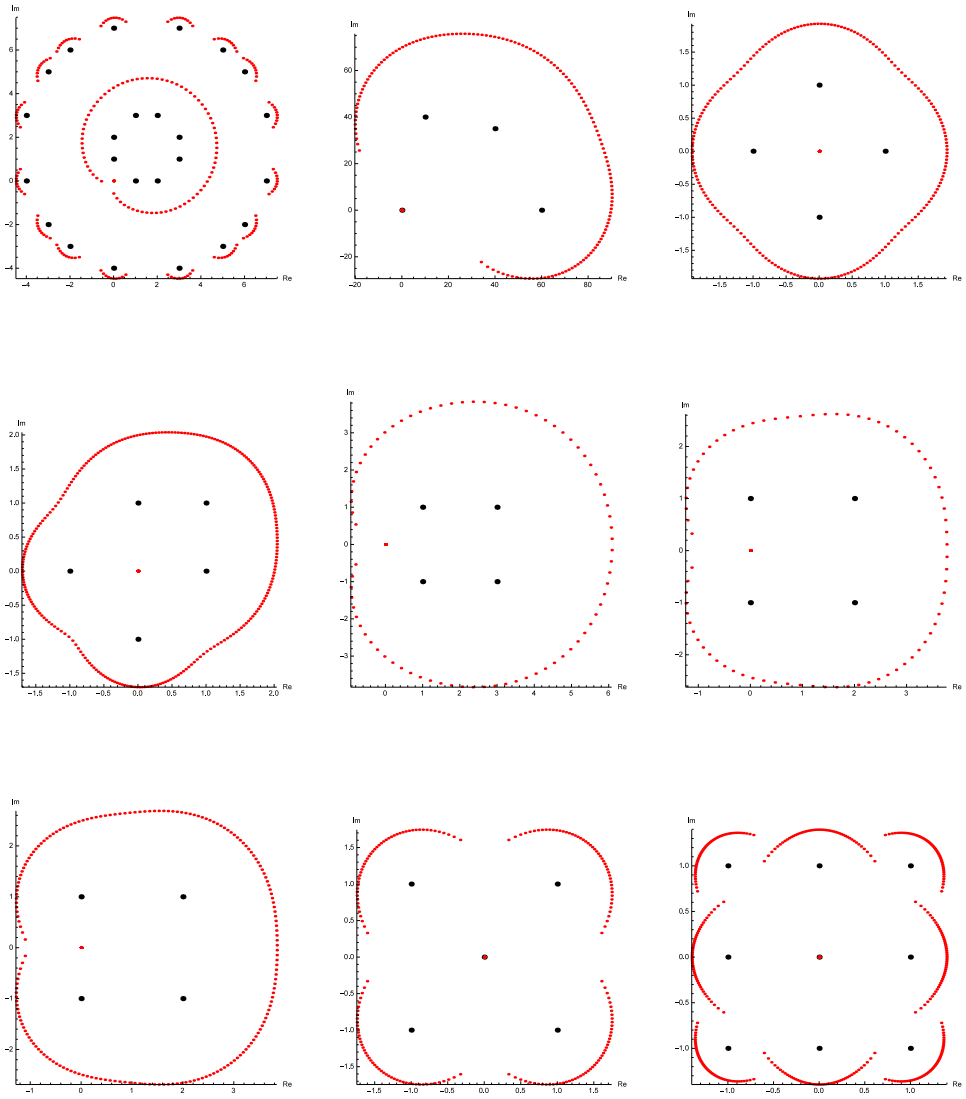

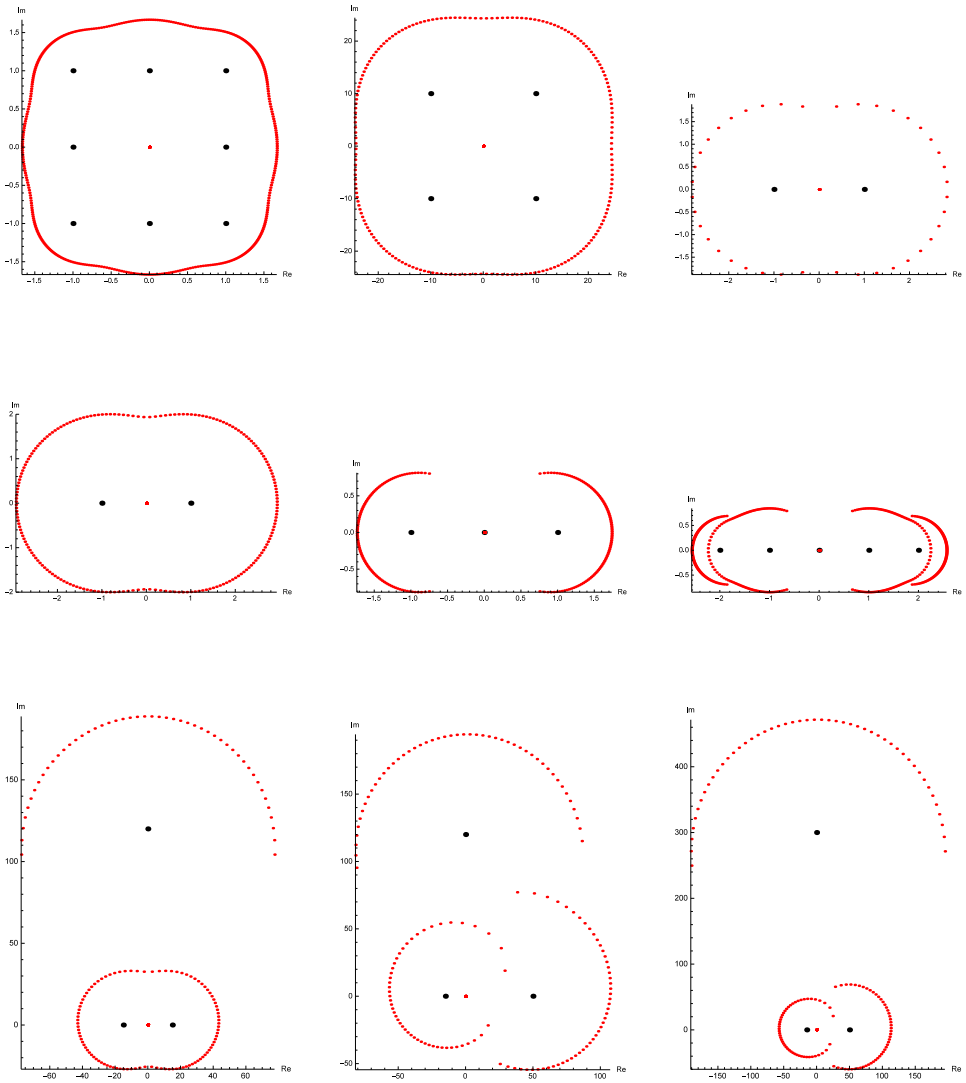
Im
Re

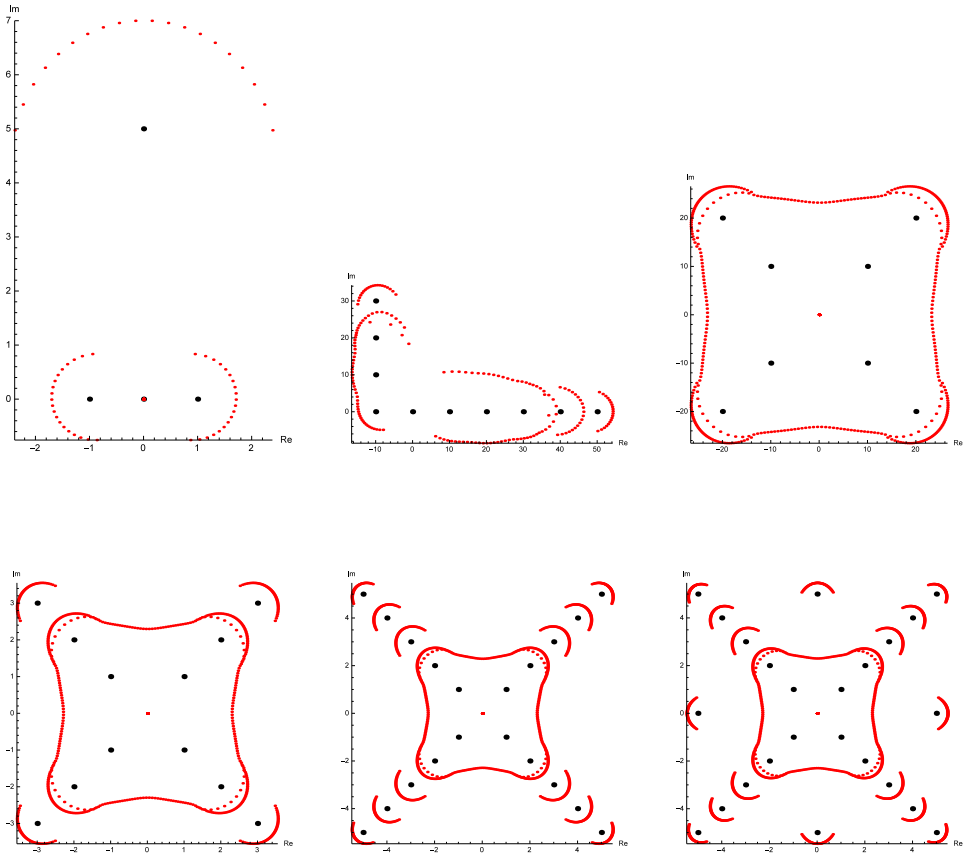
Im
Re

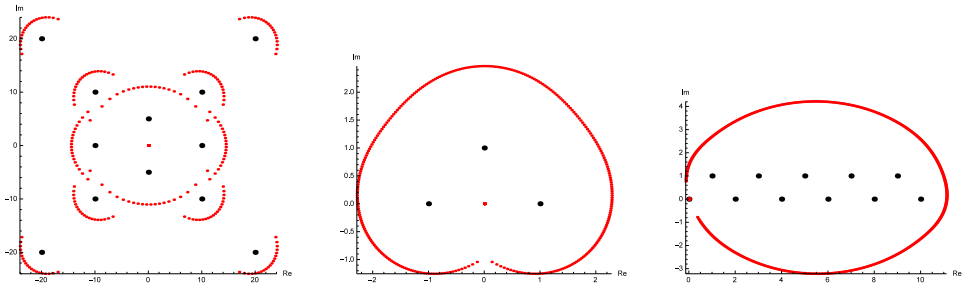

Figure 63: The zeros of $(p^n)^{(-n)}$, indicated by the red disks, for various $p$ and $n$. In each case, the black disks are the distinct, simple zeros of $p$.

# 4 Conclusions and suggestions for further research

In this paper, we have seen a connection between the Gauss-Lucas theorem and collinearity of zeros of polynomials on three separate occasions. It is likely that this connection will reveal further generalizations of the Gauss-Lucas theorem. The change of the rate (with respect to the order of the derivative) at which the convex hull of the zeros of a polynomial $p$ decreases in size, and its connection with some of the tree structures we have studied, is likely to allow further insights into the nature of such trees.

While the polynomials $(p^n)^{(n)}$ we have studied in relation to iterated forests have a great deal of mathematical elegance to them, the author is uncertain that the order of the derivative has been chosen correctly. For instance, it is unclear whether the iterated forests in figures 25 and 26 will asymptotically become a warped forest or a warped tree, assuming that either of these limiting shapes exist. It tends to be the case that slightly higher orders of the derivative clearly give rise to trees instead of forests, so it may be worthwhile to search for the smallest real constant $\kappa$ such that $(p^n)^{(\lfloor \kappa n \rfloor)}$ consistently gives rise to trees. It will likely prove fruitful to investigate the cases $1 \leq \kappa \leq 2$, and $\kappa = m/2$, where $m = \deg(p)$.

Furthermore, for any simple polygon $\mathcal{S}$ whose convex hull has $m$ vertices, we have seen an apparent maximum of $2m-3$ edges in trees associated with $\mathcal{P}(\mathcal{S})$ (see Conjecture 3.4). Figure 38 on page 42 shows that the analogous restriction for intrinsic trees is most likely false, since a triangular convex hull can give rise to (at least) four edges. Thus, it is unlikely that all of the interesting behaviors of the zero distributions of lattice polynomials are captured by intrinsic forests. Because it is unclear how to naturally define a sequence of lattice polynomials for a given shape $\mathcal{S}$, it may be more fruitful to study sequences of polynomials with $n$ zeros randomly distributed within $\mathcal{S}$, as we did on pages 20-23.

Finally, the author has two ideas for experiments that may be fruitful. First, figures 55 and 57 show that at least one rudimentary control mechanism for 'trains' of zeros exists. Other, straightforward configurations of zeros allow these trains to travel along curved paths toward zeros of high multiplicity. It is likely that further control mechanisms for these trains can be found, perhaps in order to make them travel along almost any smooth path that constantly brings them closer to the center of mass.

Second, it may be the case that tree configurations of zeros of $(p^n)^{(n)}$ exist in higher dimensions, e.g. when $p$ is a quaternion polynomial with distinct, simple zeros. Analogously to Conjecture 3.5, these trees may, given certain light restrictions, be contained in unique high-dimensional polytopes.

## References


[1] T. Bergkvist, H. Rullgård: *On polynomial eigenfunctions for a class of differential operators,* Math. Res. Lett., 9 (2002), pp. 153–171.

[2] B. Ćurgus, V. Mascioni: *A contraction of the Lucas polygon,* Proc. Amer. Math. Soc. 132 (2004), pp. 2973-2981.

[3] D.W. Farmer, R.C. Rhoades: *Differentiation evens out zero spacings,* Trans. AMS, 357(9) (2005), pp. 3789–3811.

[4] R.P. Grimaldi: *Discrete and Combinatorial Mathematics,* 5th edition, Pearson (2003).

[5] B. Gustafsson, M. Sakai: *On potential theoretic skeletons of polyhedra,* Geom. Didicata 76 (1999), pp. 1-30.

[6] M. Marden: *Geometry of Polynomials,* AMS (1966).

[7] M. Marden: *The search for a Rolle's theorem in the complex domain,* Amer. Math. Monthly, 92 (1985), pp. 643–650.

[8] V.V. Prasolov: *Polynomials,* Algorithms and Computation in Mathematics 11 (2010), DOI 10.1007/978-3-642-03980-5_1, Springer-Verlag Berlin Heidelberg.

[9] Q.I. Rahman, G. Schemisser: *Analytic Theory of Polynomials,* Oxford University Press, Oxford (2002).

[10] W. Rudin: *Real and Complex Analysis,* 3rd edition. McGraw-Hill (1987).

[11] A. Rüdinger: *Strengthening the Gauss-Lucas theorem for polynomials with Zeros in the interior of the convex hull,* arXiv:1405.0689 (2014).

[12] E.W. Weisstein: *Steiner Inellipse,* from MathWorld - A Wolfram Web Resource. `http://mathworld.wolfram.com/SteinerInellipse.html`

# Appendix A

**Definition A.1.**

1. *A collection $\tau$ of subsets of a set $X$ is said to be a topology in $X$ if $\tau$ has the following three properties:*
   (a) *$\emptyset \in \tau$ and $X \in \tau$.*
   (b) *If $V_k \in \tau$ for $k = 1, \ldots, n$, then $\bigcap_{k=1}^{n} V_k \in \tau$.*
   (c) *If $\{V_\alpha\}$ is an arbitrary collection of members of $\tau$ (finite, countable, or uncountable), then $\bigcup_\alpha V_\alpha \in \tau$.*
2. *If $\tau$ is a topology in $X$, then $X$ is called a topological space, and the members of $\tau$ are called the open sets in $X$.*
3. *If $X$ and $Y$ are topological spaces and if $f$ is a mapping of $X$ into $Y$, then $f$ is said to be continuous provided that $f^{-1}(V)$ is an open set in $X$ for every open set $V$ in $Y$.*

**Definition A.2.**

1. *A collection $\Sigma$ of subsets of a set $X$ is said to be a $\sigma$-algebra in $X$ if $\Sigma$ has the following properties:*
   (a) *$X \in \Sigma$.*
   (b) *If $A \in \Sigma$, then $A^c \in \Sigma$, where $A^c$ is the complement of $A$ relative to $X$.*
   (c) *If $A = \bigcup_{n=1}^{\infty} A_n$ and if $A_n \in \Sigma$ for $n = 1, 2, 3, \ldots$, then $A \in \Sigma$.*
2. *If $\Sigma$ is a $\sigma$-algebra in $X$, then $X$ is called a measurable space, and the members of $\Sigma$ are called the measurable sets in $X$.*
3. *If $X$ is a measurable space, $Y$ is a topological space, and $f$ is a mapping of $X$ into $Y$, then $f$ is said to be measurable provided that $f^{-1}(V)$ is a measurable set in $X$ for every open set $V$ in $Y$.*

**Definition A.3.**

1. *A positive measure is a function $\mu$, defined on a $\sigma$-algebra $\Sigma$, whose range is in $[0, \infty]$ and which is countably additive. This means that if $\{A_k\}$ is a disjoint countable collection of members of $\Sigma$, then*

$$\mu(\bigcup_{k=1}^{\infty} A_k) = \sum_{k=1}^{\infty} \mu(A_k). \tag{45}$$

   *To avoid trivialities, we shall also assume that $\mu(A) < \infty$ for at least one $A \in \Sigma$.*

2. *A measure space is a measurable space which has a positive measure defined on the $\sigma$-algebra of its measurable sets.*

3. *A complex measure is a complex-valued countably additive function defined on a $\sigma$-algebra.*

**Remark A.1.** *A positive measure is frequently referred to as a measure. Furthermore, it follows from Definition A.3 that if $\mu$ is a positive measure on a $\sigma$-algebra $\Sigma$, then $\mu(\emptyset) = 0$.*

**Definition A.4.** *The support of a complex function $f$ on a topological space $X$ is the closure of the set $\{x : f(x) \neq 0\}$.*

**Definition A.5.** *Let $V$ be a finite nonempty set, and let $E \subseteq V \times V$. The pair $(V, E)$ is then called a directed graph (on $V$), or digraph (on $V$), where $V$ is the set of vertices, or nodes, and $E$ is its set of (directed) edges or arcs. We write $G = (V, E)$ to denote such a graph.*

*When there is no concern about the direction of any edge, we still write $G = (V, E)$. But now $E$ is a set of unordered pairs of elements taken from $V$, and $G$ is called an undirected graph.*

**Remark A.2.** *If we say that $G$ is a graph, it is implied that $G$ is an undirected graph.*

**Definition A.6.** *Let $G = (V, E)$ be a graph with $a \in V$. An edge $(a, a) \in E$ is called a loop. If $G$ has no loops, it is said to be loop-free.*

**Definition A.7.** *Let $x$, $y$ be (not necessarily distinct) vertices in a graph $G = (V, E)$. An $x - y$ walk in $G$ is a (loop-free) finite alternating sequence*

$$x = x_0,\, e_1,\, x_1\, e_2,\, x_2,\, e_3, \ldots, e_{n-1},\, x_{n-1},\, e_n,\, x_n = y$$

*of vertices and edges from $G$, starting at vertex $x$ and ending at vertex $y$ and involving the $n$ edges $e_i = (x_{i-1},\, x_i)$, where $1 \leq i \leq n$.*

*The length of this walk is $n$, the number of edges in the walk. Any $x - y$ walk where $x = y$ (and $n > 1$) is called a closed walk. Otherwise the walk is called open.*

**Definition A.8.** *Consider any $x - y$ walk in a graph $G = (V, E)$.*

1. *If no edge in the $x - y$ walk is repeated, then the walk is called an $x - y$ trail. A closed $x - x$ trail is called a circuit.*

2. *If no vertex of the $x - y$ walk occurs more than once, then the walk is called an $x - y$ path. When $x = y$, the term cycle is used to describe such a closed path.*

**Definition A.9.** *Let $G = (V, E)$ be an undirected graph. We call $G$ connected if there is a path between any two distinct vertices of $G$.*

*Let $G = (V, E)$ be a directed graph. Its associated undirected graph is the graph obtained from $G$ by ignoring the directions on the edges. If more than one undirected edge results for a pair of distinct vertices in $G$, then only one of these edges is drawn in the associated undirected graph. When this associated graph is connected, we consider $G$ connected.*

*A graph that is not connected is called disconnected.*

**Definition A.10.** *A graph $G$ is called planar if $G$ can be drawn in the plane with its edges intersecting only at vertices of $G$. Such a drawing of $G$ is called an embedding of $G$ in the plane.*

**Definition A.11.** *Let $G = (V, E)$ be an graph. For each vertex $v \in V$, the degree of $v$, written $\deg(v)$, is the number of edges in $G$ that are incident with $v$. Here a loop at a vertex $v$ is considered as two incident edges for $v$.*

**Definition A.12.** *Let $G = (V, E)$ be a loop-free, undirected graph. The graph $G$ is called a forest if $G$ contains no cycles. A forest that is connected is called a tree.*

**Definition A.13.** *Let $T = (V, E)$ be a tree. A vertex $v \in V$ with $\deg(v) = 1$ is called a leaf vertex.*

**Theorem A.1.** *The critical points of a polynomial $P$ which are not multiple zeros of $P$ are located at the equilibrium positions in a certain field of force. This field is one due to a particle placed at each zero of $P$, having a mass equal to the multiplicity of the zero and attracting according to the inverse distance law.*

**Theorem A.2.** *If $P : \mathbb{C} \to \mathbb{C}$ is a non-constant polynomial, there exists a complex number $\lambda$ such that $P(\lambda) = 0$.*

For convenience, it is desirable to generalize the product rule in calculus ($(fg)' = f'g + fg'$) to handle the $n$:th derivative of a product of $m$ differentiable functions. We begin with the case $m = 2$.

**Theorem A.3.** *Let $f$ and $g$ be $n$ times differentiable $\mathbb{C} \to \mathbb{C}$ functions. Then*

$$(fg)^{(n)} = \sum_{k=0}^{n} \binom{n}{k} f^{(k)} g^{(n-k)}. \tag{46}$$

*Proof.* We will use proof by induction. Obviously, equation (46) is valid for $n = 0$. The product rule yields

$$(fg)' = f'g + fg' = \sum_{k=0}^{1} \binom{1}{k} f^{(k)} g^{(1-k)}, \tag{47}$$

which shows (46) is valid for $n = 1$ as well. Assume that (46) is valid when $n = m$, for some fixed integer $m \geq 1$; that is

$$(fg)^{(m)} = \sum_{k=0}^{m} \binom{m}{k} f^{(k)} g^{(m-k)}. \tag{48}$$

When $n = m + 1$, we see that

$$\begin{aligned}
(fg)^{(m+1)} &= \Big((fg)^{(m)}\Big)' = \text{[equation (48)]} = \left(\sum_{k=0}^{m} \binom{m}{k} f^{(k)} g^{(m-k)}\right)' \\
&= \sum_{k=0}^{m} \binom{m}{k} \left(f^{(k+1)} g^{(m-k)} + f^{(k)} g^{(m+1-k)}\right) \\
&= \sum_{k=1}^{m+1} \binom{m}{k-1} f^{(k)} g^{(m+1-k)} + \sum_{k=0}^{m} \binom{m}{k} f^{(k)} g^{(m+1-k)} \\
&= \binom{m}{m+1-1} f^{(m+1)} g^{(m+1-(m+1))} + \binom{m}{0} f^{(0)} g^{(m+1)} \\
&+ \sum_{k=1}^{m} \left[\binom{m}{k-1} + \binom{m}{k}\right] f^{(k)} g^{(m+1-k)} \\
&= f^{(m+1)} g + f g^{(m+1)} + \sum_{k=1}^{m} \binom{m+1}{k} f^{(k)} g^{(m+1-k)} \\
&= \sum_{k=0}^{m+1} \binom{m+1}{k} f^{(k)} g^{(m+1-k)}.
\end{aligned} \tag{49}$$

Thus, equation (46) is valid for $n = m + 1$, and the theorem follows by mathematical induction. □

Equation (46) is sometimes referred to as the general Leibniz rule. We are now ready to generalize this rule further.

**Theorem A.4.** *Let $f_1, f_2, \ldots, f_m$ be $n$ times differentiable $\mathbb{C} \to \mathbb{C}$ functions. Then*

$$(f_1 f_2 \cdots f_m)^{(n)} = \sum_{k_1+k_2+\cdots+k_m=n} \binom{n}{k_1, k_2, \ldots, k_m} \prod_{t=1}^{m} f_t^{(k_t)}, \tag{50}$$

*where $k_1, k_2, \ldots, k_m$ are nonnegative integers.*

*Proof.* We will use proof by induction over the number of functions. When $m = 2$, equation (50) is identical with equation (46) in Theorem A.3. Assume that (50) is valid when $m = r$, for some fixed integer $r \geq 2$. When $m = r+1$, equation (46), immediately followed by the inductive assumption, yield

$$\begin{aligned}
(f_1 f_2 \cdots f_{r+1})^{(n)} &= \left( f_{r+1} \prod_{t=1}^{r} f_t \right)^{(n)} \\
&= \sum_{k_{r+1}=0}^{n} \binom{n}{k_{r+1}} f_{r+1}^{(k_{r+1})} \cdot \left( \prod_{t=1}^{r} f_t \right)^{(n-k_{r+1})} \\
&= \sum_{k_{r+1}=0}^{n} \binom{n}{k_{r+1}} f_{r+1}^{(k_{r+1})} \cdot \sum_{k_1+\cdots+k_r=n-k_{r+1}} \binom{n-k_{r+1}}{k_1, \ldots, k_r} \prod_{t=1}^{r} f_t^{(k_t)} \\
&= \sum_{k_{r+1}=0}^{n} \sum_{k_1+\cdots+k_r=n-k_{r+1}} \binom{n}{k_1, \ldots, k_r, k_{r+1}} f_{r+1}^{(k_{r+1})} \cdot \prod_{t=1}^{r} f_t^{(k_t)} \\
&= \sum_{k_1+\cdots+k_r+k_{r+1}=n} \binom{n}{k_1, \ldots, k_r, k_{r+1}} \prod_{t=1}^{r+1} f_t^{(k_t)}.
\end{aligned} \tag{51}$$

It follows from (51) that (50) is valid for $m = r + 1$. The theorem follows by mathematical induction. □